UNIVERSITAT POLITÈCNICA DE VALÈNCIA

Escuela Técnica Superior de Ingeniería del Diseño

Comparative study of three electrochemical cell models for the CFD simulation of a battery module

Aerospace Engineering Bachelor Thesis

Valencia, July 15, 2021

Author:
Vanaclocha Hervás, Carlos

Supervisors:
Margot, Xandra Marcelle
Arcila, Arturo

Abstract

In this project a comparative study of the responses of three different electrochemical models for a simulation of a battery module will be carried out in ANSYS. For this purpose, each model will be subjected to several charge and discharge processes and then the responses of some characteristic variables of a battery will be compared, with the objective of examining the behaviour of each one of the models. In the first place, a series of simple discharges at different C-rates will be applied. Next, a compound cycle with several charge/discharge intervals will be introduced, and finally the impact of the determination of the model parameters will be assessed through another series of simple discharges. To perform the comparison between the models, both the evolution of the studied variables and the computation time will be taken into account, as well as other remarkable factors that may appear during the course of the simulations.

En el presente trabajo se realizará en ANSYS un estudio comparativo de la respuesta de tres modelos electroquímicos diferentes para una simulación de un módulo de baterías. Para ello, cada modelo se someterá a diversos procesos de carga y descarga preestablecidos y posteriormente se compararán las respuestas de variables características de una batería con el objetivo de examinar el comportamiento de cada uno de los modelos. En primer lugar, se aplicarán una serie de descargas simples a diferentes C-rates. A continuación, se introducirá un ciclo compuesto con varios intervalos de carga/descarga y finalmente se comprobará el impacto de la determinación de los parámetros de uno de los modelos mediante otra serie de descargas simples. Para llevar a cabo la comparación entre los modelos, se tendrán en cuenta tanto la evolución de las variables estudiadas como el tiempo de computación, así como otros factores relevantes que puedan aparecer en el transcurso de las simulaciones.

En el present treball es realitzarà en ANSYS un estudi comparatiu de la resposta de tres models electroquímics diferents per a una simulació d'un mòdul de bateries. Per a fer-ho, cada model es sotmetrà a diversos procesos preestablerts de càrrega i descàrrega i posteriorment es compararan les respostes de variables característiques d'una bateria amb l'objectiu d'examinar el comportament de cadascun dels models. En primer lloc s'aplicaran una serie de descàrregues simples a diferents C-rates. A continuació s'introduirà un cicle compost amb diversos intervals de càrrega/descàrrega i finalment es comprovarà l'impacte de la determinació dels paràmetres d'un dels models mitjançant una altra sèrie de descàrregues simples. Per a dur a terme la comparació entre els models, es tindran en compte tant l'evolució de les variables estudiades com el temps de computació, així com altres factors rellevants que puguen aparéixer en el transcurs de les simulacions.

Contents

---

0. Nomenclature

α_a	Charge transfer coefficient at anode
α_c	Charge transfer coefficient at cathode
β	Bruggeman porosity exponent
$\dot{q}_{abuse}$	Heat generation due to thermal runaway reactions under thermal abuse condition
$\dot{q}_{ECh}$	Electrochemical reaction heat due to electrochemical reactions
$\dot{q}_{short}$	Heat generation rate due to internal short-circuit
η	Overpotential
ρ	Density
σ^{eff}	Effective electric conductivity
σ_+	Effective electric conductivity for the positive electrode
σ_-	Effective electric conductivity for the negative electrode
ε_e	Volume fraction of the electrolyte phase in electrode
ε_f	Volume fraction of filler material in electrode
ε_s	Volume fraction of the active material in electrode
φ_+	Phase potential for the positive electrode
φ_-	Phase potential for the negative electrode
a_s	Solid/electrolyte interfacial area per unit volume
C	Capacitance
c_e	Electrolyte phase concentration
C_p	Heat capacity at constant pressure
c_s	Solid (electrode) phase concentration
D_e	Diffusion coefficient of Li+ in the electrolyte phase
D_s	Diffusion coefficient of Li in solid
$D_{s,ref}$	Reference solid diffusion coefficient
DoD	Depth of discharge
E_d	Activation energy that controls the temperature sensitivity of D_s
E_r	Activation energy that controls the temperature sensitivity of k_m
F	Faraday constant
$f_\pm$	Electrolyte activity coefficient

I	Electric current
i_0	Exchange current density
i_p	Transverse current density
j_{ECh}	Volumetric current transfer rate due to electrochemical reactions
j_{short}	Volumetric current transfer rate due to internal short-circuit
k	Electrolyte ionic conductivity (2.20)
k	Thermal conductivity (2.1)
k_D^{eff}	Electrolyte diffusional conductivity
$k_{m,ref}$	Reference solid reaction rate constant
l_n	Negative electrode thickness
l_p	Positive electrode thickness
l_s	Separator thickness
$Q_{nominal}$	Battery total electric capacity
Q_{ref}	Battery capacity used in experiments
R	Resistance (Section 2.3.2)
R	Universal gas constant (Section 2.3.3)
SOC	State of charge
T	Temperature
t	Time
t_+^0	Transference number of lithium ion
T_{ref}	reference temperature (298 K)
U	Open circuit potential of an electrode reaction
V	Battery cell voltage
V_{OCV}	Open circuit voltage
Vol	Active zone volume of a single battery

1. Objective and scope of the thesis

The growing concern for the environmental situation of our planet has put many industries in a challenging position, where they are to find cleaner, more sustainable alternatives to the damaging and ever more limited sources of energy that have been exploited so far. One of these industries that have been brought under the spotlight is transportation, accountable for up to 49% of the usage of global oil resources [2] and object of regulation from administrations worldwide because of its considerable contribution to total CO_2 emissions.

In recent years, a seemingly increasing skepticism has surrounded diesel engines, partly as a result from the economic discouragement imposed by many governments. Petrol engines too are making a gradual exit, making way for other kinds of vehicles, namely hybrid electrical vehicles (HEV) and purely electrical ones (EV), upon which a powerful economic support is being placed. Even if their introduction has been slow, the number of HEVs and EVs available in the market grows every year, and so does their quality, having reached the point where their general performance is similar and even greater than that of a fuel-powered car in some cases. The challenge of energy storage is still the subject of intensive ongoing investigation, motivated by automotive manufacturers such as Tesla [15] and BMW [20], who intend to release high-performance EVs in the near future, proving that there are means and resources to induce a shift in the market from fossil fuels towards clean electrical energy.

The reason why the introduction of electrical engines has been relatively unaccelerated is due to the fact that there are still concerns on the safety and the capability of storage of the batteries [9]. In the past, several types of batteries have been tested and successfully introduced in HEVs and EVs: nickel-metal hydride batteries (NiMH), nickel-cadmium (NiCd) or lead-acid to name a few, but the one type that is most common in the latest applications because of its higher performance capability and efficiency are lithium-ion batteries (LIB). These have generally greater energy density and therefore take up less space and weight than their counterparts [10]. They also allow for a longer range between charges, with just a slightly higher cost. The main challenge regarding LIBs is the control of their temperature. If the cell gets too hot, there is an elevated risk of thermal runaway, characterised by the appearance of highly exothermic reactions within the cell, leading to an even further generation of heat and eventually to an explosive decomposition [26**?**]. On the other hand, if the cell is required to perform in sub-zero temperature conditions, its discharge capacity will be noticeably affected, reducing its range and efficiency greatly [26]. This is the reason why the implementation of LIBs comes with the added cost of having to provide a thermal management system (TMS) that takes care of these issues, normally by forcing a convection in a fluid that will exchange heat with the walls of the cell or by introducing a phase change material (PCM) with a very high latent heat [7].

To carry out a proper analysis of the behaviour of a battery by simulation with a CFD software like ANSYS, an appropriate model must be used, one that resembles closely the electrochemical performance of the actual battery cell. That is why in this thesis a comparison between three models available in ANSYS Fluent will be carried out, taking into consideration their time efficiency and possible biases and deficient responses to the given requirements.

2. Introduction

2.1 Working principles of a Li-ion battery

The term lithium-ion battery refers to a family of rechargeable batteries in which there is a flow of lithium ions (Li+) between the two electrodes [21]. The basic mechanism is shown in Figure 2.1. During the discharge, the positive lithium ions move from the negative electrode (anode) to the positive electrode (cathode) through an electrolyte solution and a separator, and vice versa during the charging process.

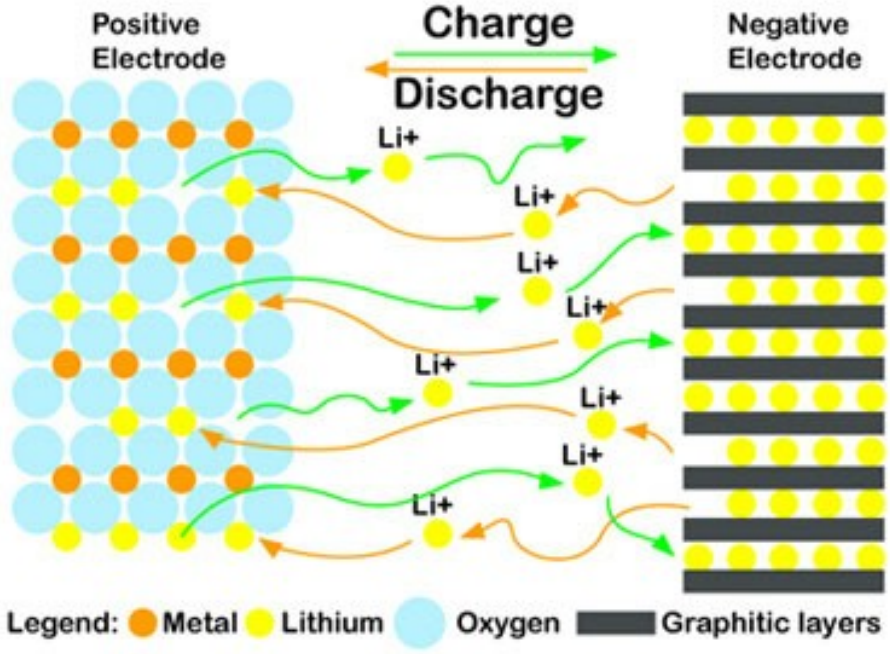

Figure 2.1: Mechanism of a Li-ion battery during charge and discharge, adapted from [26]

The anode is usually made of a carbon material, being graphite the most popular option because of its low working potential [13], even though there are other less widespread batteries that have titanium compounds (lithium-titanate-oxide or LTO batteries) or silicone based materials (nanowire batteries) as anodes. These are all used because of its availability, electrical conductivity and ability to intercalate lithium ions in its structure.

The cathode, on the other hand, is made of a lithium-containing compound that is generally a layered oxide, a spinel or a polyanion. The most widely used are cobalt-based cathodes ($LiCoO_2$), which fall under the layered oxide category. It is ideal due to its high energy density, good cyclic performance and many other advantageous properties, even if its costly price and low thermal stability constitute two limiting factors to it. As of today, iron-based polyanions ($LiFePO_4$) are being introduced as a cheaper alternative to its more efficient cobalt-based counterparts. They have proven to have a good cycle durability and safety, but its power density is significantly lower [16, 19, 22].

An example of the chemical reactions taking place in the electrodes are the following [26]:

Anode:

$\text{Li}_x C_6 \iff Li_0 C_6 + xLi^+ + xe^-$

Cathode:

$\text{Li}_{y-x} Mn_2 O_4 + xLi^+ + xe^- \iff Li_y Mn_2 O_4$

In these reactions, the left side of the expression corresponds to the charged state of the battery, in which the lithium ions are located in the cathode, and the right one to the discharged state, in which they move to the anode.

The electrolyte is the medium through which the ions migrate from one electrode to the other. Liquid electrolytes consist of lithium salts, most commonly hexafluorophosphate ($LiPF_6$) in an organic solvent such as ethylene carbonate [27]. Solid electrolytes are a product of recent investigation, allowing a steady transport of lithium ions without the risk of leaks. The most promising type are ceramics, mainly lithium metal oxides.

Also between the two electrodes lies the separator. It is generally a permeable membrane whose function is to keep the anode and the cathode separated to prevent electrical short circuits while allowing the transfer of ionic charge carriers to create an electric current. Ethylene, polyethylene and polypropylene are some materials that can be found in commercially available separators.

Each electrode has an associated current collector, which assembles the electrical energy to exchange it with the motor. The collector of the anode is usually made of copper, and the one in the cathode is made of aluminium. The energy loss associated with the contact between electrode and collector can be prominent, as high as 20% under typical operating conditions [23].

There are several configurations in which lithium-ion battery cells can be found, the most common of them are shown in Figure 2.2. Individual battery cells can be grouped together to form battery modules, and in turn battery packs, which are used for purposes that need substantial amounts of energy. For vehicle applications, the prismatic type has been proven to be the most effective due to its superior cooling ability. In the past, cylindrical cells have been used because of its cost, safety and availability, and even if prismatic-type batteries have taken the lead in most current applications, they are still implemented in vehicles such as Tesla Model S (Figure 2.3) and Tesla Model X [26].

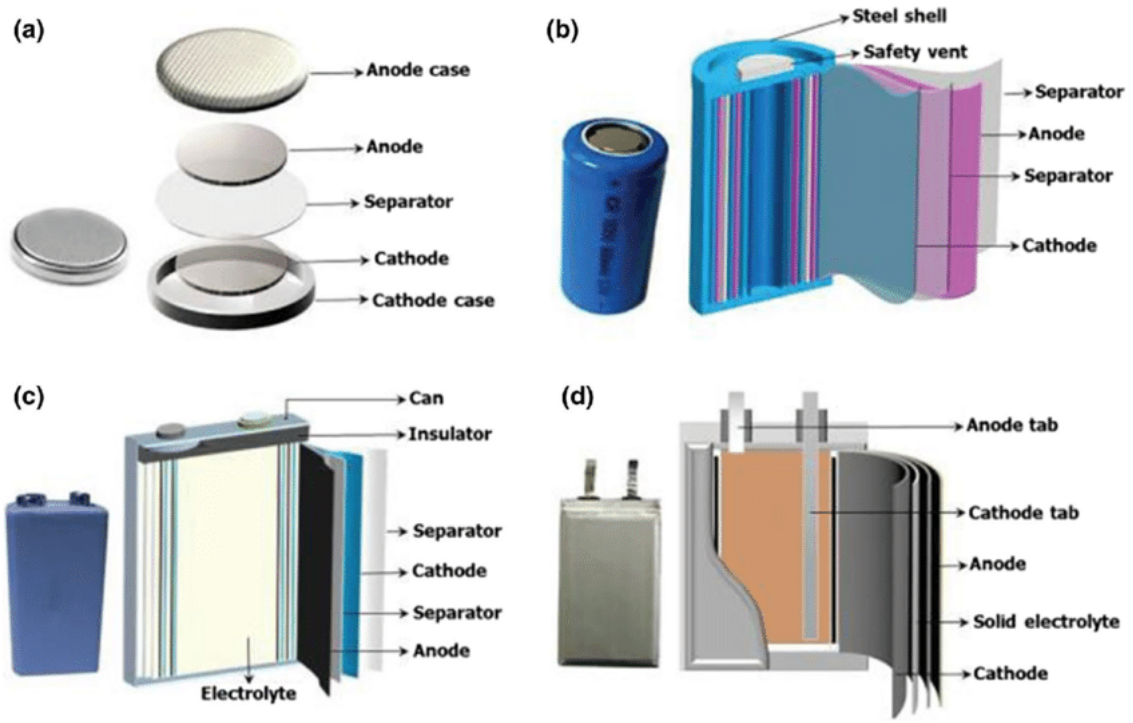

Figure 2.2: Battery cell configurations types: (a) coin (b) cylindrical (c) prismatic and (d) pouch [1]

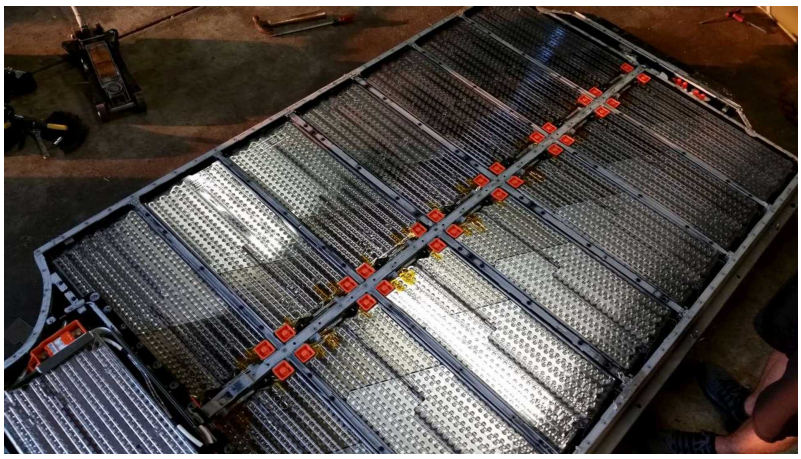

Figure 2.3: Battery pack of a Tesla Model S [11]

2.2 TOSHIBA SCiB^{TM} battery cell

The battery that will be object of study in this paper will be a TOSHIBA SCiB^{TM} (Figure 2.4). It is a lithium titanate (LTO) rechargable battery the name of which stands for "Super Charge Ion Battery", since it can be charged to 90% in as little as 10 minutes. It has a capacity of 23 A·h and a nominal voltage of 2.3 V, and it presents the following significant characteristics [25]:

- Low risk of fire or explosion. In case of internal short circuit, the lithium titanium oxide in the anode acquires a high resistance, minimising the possibility of overheating.
- Usable lifespan of at least 20.000 cycles with small capacity degradation.

- Charge of 80% of capacity in 6 minutes, which allows vehicles to charge almost as fast as a gasoline engine. Furthermore, rapid charging does not cause notable deterioration in capacity.
- High power input/output in a short period of time, due to the high current charge and discharge. This makes possible the efficient storage of the braking energy of a vehicle, and also the starting of a motor without external aid.
- Performance at low temperatures of up to -30^{o}C, since the lithium metal does not precipitate.
- Wide effective SOC range of 0% to 100% with good input/output characteristics. This allows for the reduction of battery cells mounted in a system.

Figure 2.4: Toshiba SCiB^{TM} battery cell

SCiB^{TM} batteries have been implemented in several systems, such as a prototype laptop by Toshiba, the Schwinn Tailwind electric bike and Honda's EV-neo electric bike. While its use in automobiles is still quite limited, it can be found in the Japanese version of Mitsubishi's i-MiEV and Minicab MiEV and in Honda's Fit EV.

In Figure 2.5 the dimensions of the battery cell are shown.

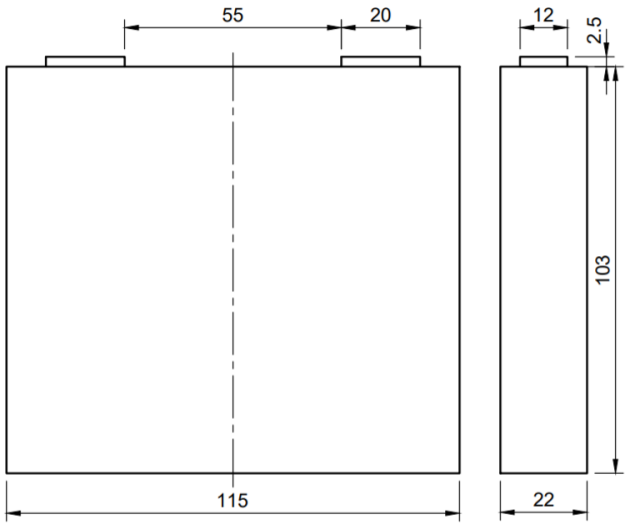

Figure 2.5: Toshiba SCiB^{TM} battery cell dimensions in mm

2.3 Models of battery simulation in ANSYS

For the purpose of performing simulations, four different solution methods are available in ANSYS Fluent in the version 2020 R2, each one with a different thermal-electrochemical coupling [4]:

- CHT coupling method
- FMU-CHT coupling method
- Circuit Network solution method
- MSMD solution method

The one that will be used in the simulation of the battery is the Multi-Scale Multi-Domain (MSMD) approach, since it is capable to resolve the electro-chemical phenomena taking place in a system with complex geometry and diverse physical properties.

The thermal and electrical fields are solved with the following equations:

$$\frac{\partial \rho C_p T}{\partial t} - \nabla \cdot (k \nabla T) = \sigma_+ \mid \nabla \phi_+ \mid^2 + \sigma_- \mid \nabla \phi_- \mid^2 + \dot{q}_{ECh} + \dot{q}_{short} + \dot{q}_{abuse} \tag{2.1}$$

$$\begin{aligned} \nabla \cdot (\sigma_+ \nabla \varphi_+) &= -(j_{ECh} - j_{short}) \\ \nabla \cdot (\sigma_- \nabla \varphi_-) &= j_{ECh} - j_{short} \end{aligned} \tag{2.2}$$

Equation 2.1 can be identified as an equation of energy and the set 2.2 corresponds to the equations of potential, which is solved only in the active zones of the cell.

Using this method, a multitude of models can be found in literature, and even custom ones can be implemented in FLUENT. The available electrochemical models that are available in ANSYS are the following:

- Newman, Tiedemann, Gu and Kim (NTGK) model
- Equivalent Circuit Model (ECM)
- Newman Pseudo-2D (P2D) model

2.3.1. NTGK model

The Newman, Tiedemann, Gu and Kim (NTGK) model is a simple semi-empirical electro-chemical model. In this model, the volumetric current transfer rate (j_{ECh}) is calculated with the following expression:

$$j_{ECh} = \frac{Q_{nominal}}{Q_{ref} Vol} Y [U - V] \tag{2.3}$$

where Y and U are parameters that are a function of the battery depth of discharge (DoD).

$$DoD = \frac{Vol}{3600 Q_{nominal}} \int_0^t j \, dt \tag{2.4}$$

$$U = (\sum_{n=0}^{5} a_n (DoD)^n) - C_2(T - T_{ref}) \tag{2.5}$$

$$Y = (\sum_{n=0}^{5} b_n (DoD)^n) exp[-C_1(\frac{1}{T} - \frac{1}{T_{ref}})] \tag{2.6}$$

C_1 and C_2 are the battery specific NTGK model constants.

The electrochemical reaction heat $\dot{q}_{ECh}$ of equations 2.1 and 2.2 is calculated as

$$\dot{q}_{ECh} = j_{ECh}[U - V - T\frac{dU}{dT}] \tag{2.7}$$

The NTGK model is accurate in charge/discharge cycles in which the electric load presents no abrupt changes. If there are sudden shifts in the electric load, it will not account for the inertial changes and other models such as ECM will be more precise.

2.3.2. ECM model

The Equivalent Circuit Model is a semi-empirical model as well, in which an electrical circuit simulates the electric behaviour of the battery [5, 18]. The second order circuit that will be employed consists of three resistors and two capacitors, as can be seen in Figure 2.6

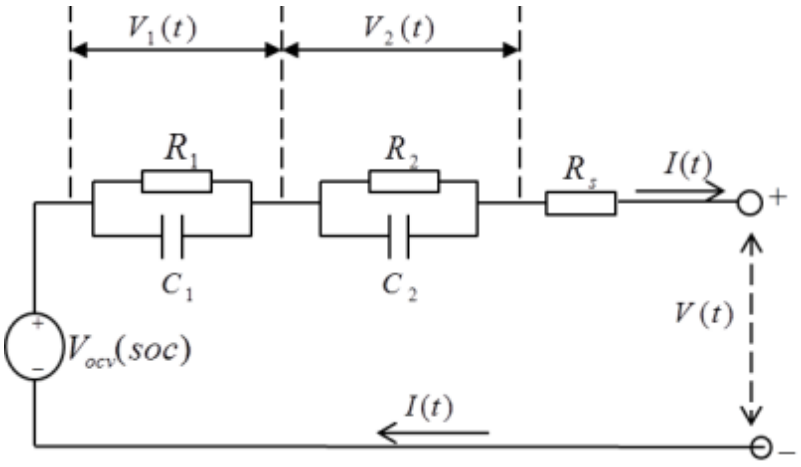

Figure 2.6: ECM model electrical circuit

The voltage-current relation can be obtained by solving the electric circuit equations:

$$\begin{aligned} V &= V_{OCV}(soc) - V_1 - V_2 - R_S(soc)I(t) \\ \frac{dV_1}{dt} &= -\frac{1}{R_1(soc)C_1(soc)}V_1 - \frac{1}{C_1(soc)}I(t) \\ \frac{dV_2}{dt} &= -\frac{1}{R_2(soc)C_2(soc)}V_2 - \frac{1}{C_2(soc)}I(t) \\ \frac{d(soc)}{dt} &= \frac{I(t)}{3600Q_{ref}} \end{aligned} \tag{2.8}$$

For a given system, the rest of the six variables (three resistances, two capacitances and the open circuit voltage) can be expressed in three different ways as a function of the state of charge (SOC) and/or temperature:

1. With fifth order polynomials:

$$\begin{aligned} R_S &= a_0 + a_1(soc) + a_2(soc)^2 + a_3(soc)^3 + a_4(soc)^4 + a_5(soc)^5 \\ R_1 &= b_0 + b_1(soc) + b_2(soc)^2 + b_3(soc)^3 + b_4(soc)^4 + b_5(soc)^5 \\ C_1 &= c_0 + c_1(soc) + c_2(soc)^2 + c_3(soc)^3 + c_4(soc)^4 + c_5(soc)^5 \\ R_2 &= d_0 + d_1(soc) + d_2(soc)^2 + d_3(soc)^3 + d_4(soc)^4 + d_5(soc)^5 \\ C_2 &= e_0 + e_1(soc) + e_2(soc)^2 + e_3(soc)^3 + e_4(soc)^4 + e_5(soc)^5 \\ V_{OCV} &= f_0 + f_1(soc) + f_2(soc)^2 + f_3(soc)^3 + f_4(soc)^4 + f_5(soc)^5 \end{aligned} \tag{2.9}$$

2. With a function form proposed by Chen [18]:

$$\begin{aligned} R_S &= a_0 + a_1 exp[-a_2(soc)] \\ R_1 &= b_0 + b_1 exp[-b_2(soc)] \\ C_1 &= c_0 + c_1 exp[-c_2(soc)] \\ R_2 &= d_0 + d_1 exp[-d_2(soc)] \\ C_2 &= e_0 + e_1 exp[-e_2(soc)] \\ V_{OCV} &= f_0 + f_1(soc) + f_2(soc)^2 + f_3(soc)^3 + f_4 exp[-f_5(soc)] \end{aligned} \tag{2.10}$$

3. With a 2D table that defines each parameter as a function of SOC and temperature. Note that this is the only form in which the effect of temperature is directly considered.

In this model, the source terms in equations 2.1 and 2.2 are computed as:

$$j_{ECh} = I \frac{Q_{Nominal}}{Q_{ref} Vol} \tag{2.11}$$

$$\dot{q}_{ECh} = j_{ECh}[V_{OCV} - V - T\frac{dU}{dT}] \tag{2.12}$$

The ECM model is economical and very versatile at the same time, valid for batteries of many sorts, not only Li-ion.

2.3.3. P2D model

The Pseudo-2D model is a physics-based model developed by Newman's group using a porous electrode and concentrated solution theory that comprehensively mimics the transit of lithium ions in the battery [17, 5, 12].

In this model, the electrodes are a composite created by the electrolyte and active material. The electrolyte is continuous across the negative electrode, the separator and the positive electrode, whereas the solid phase, modeled as a matrix of spheres, is present only in the electrodes (Figure 2.7).

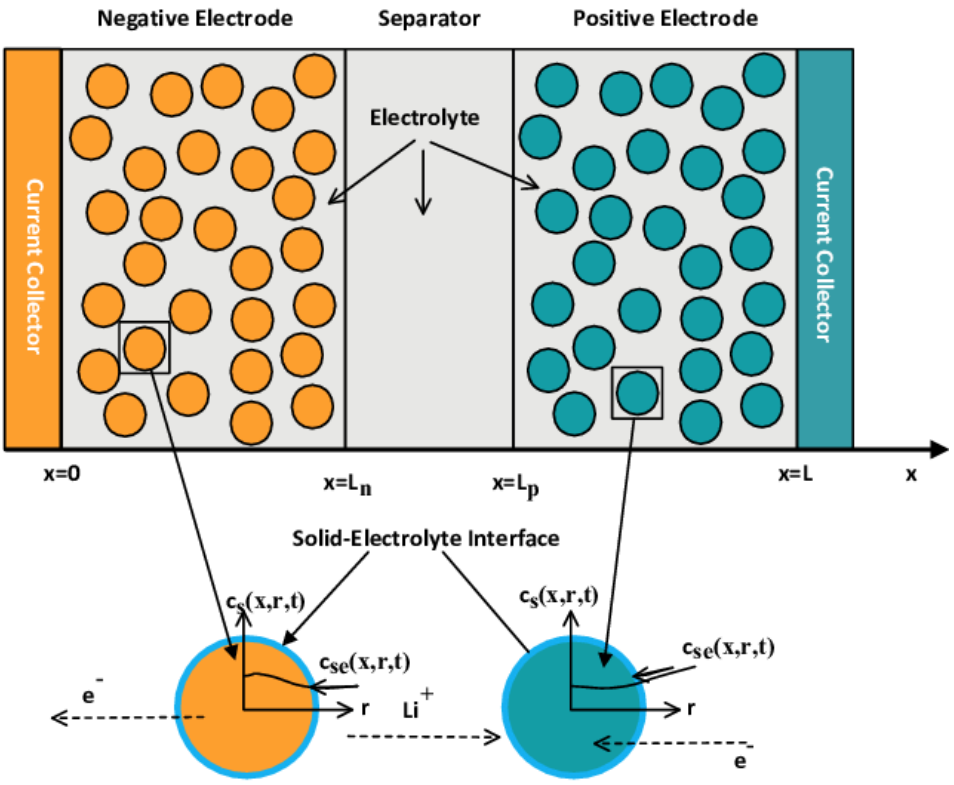

Figure 2.7: P2D model, adapted from [8]

During the discharge process, each active material sphere in the negative electrode releases lithium ions and electrons through its surface. These are carried by diffusion through the electrolyte to the positive electrode, where they are stored inside the spheres of the positive electrode until a charging operation causes an analogous process where ions migrate in the opposite direction.

The transport of lithium ions through the porous electrolyte is modeled with the charge and mass conservation laws. The first one governs the phase potentials and the second one, the phase concentrations. In the spheres, the Lithium conservation equation is solved with the r-dimension as coordinate, that is why this model is widely referred as a pseudo-2D model. The equations that describe the process are the following:

Lithium conservation in the solid phase:

$$\frac{\partial c_s}{\partial t} = \frac{D_s}{r^2}\frac{\partial}{\partial r}(r^2\frac{\partial c_s}{\partial r}) \tag{2.13}$$

Lithium conservation in the electrolyte phase:

$$\frac{\partial \varepsilon_e c_e}{\partial t} = \frac{\partial}{\partial x}(D_e^{eff}\frac{\partial c_e}{\partial x}) + \frac{1-t_+^0}{F}j^{Li} \tag{2.14}$$

Charge conservation in the solid phase:

$$\frac{\partial}{\partial x}(\sigma^{eff}\frac{\partial \varphi_s}{\partial x}) - j^{Li} = 0 \tag{2.15}$$

Charge conservation in the electrolyte phase:

$$\frac{\partial}{\partial x}(k^{eff}\frac{\partial \varphi_e}{\partial x}) + \frac{\partial}{\partial x}(k_D^{eff}\frac{\partial lnc_e}{\partial x}) + j^{Li} = 0 \tag{2.16}$$

The Butler-Volmer equation, which couples the charge and mass equations:

$$j^{Li} = a_s i_0\{exp(\frac{\alpha_a F}{RT}\eta) - exp(-\frac{\alpha_c F}{RT}\eta)\} \tag{2.17}$$

where η (overpotential) is defined as:

$$\eta = \varphi_s - \varphi_e - U \tag{2.18}$$

and i_0 is the current density, defined as:

$$i_0 = k_m(c_e)^{\alpha_a}(C_{s,max} - c_{s,e})^{\alpha_a}(c_{s,e})^{\alpha_c} \tag{2.19}$$

The effective properties used in these equations are defined as:

$$\begin{aligned} D_e^{eff} &= D_e\varepsilon_e^{\beta} \\ k^{eff} &= k\varepsilon_e^{\beta} \\ k_D^{eff} &= \frac{2RTk^{eff}}{F}(t_+^0 - 1)(1 + \frac{dlnf_{\pm}}{dlnc_e}) \\ \sigma^{eff} &= \sigma\varepsilon_s^{\beta} \\ a_s &= 3\varepsilon_s/r_s \\ D_s &= D_{s,ref}exp[-E_d/R(1/T - 1/T_{ref})] \\ k_m &= k_{m,ref}exp[-E_r/R(1/T - 1/T_{ref})] \end{aligned} \tag{2.20}$$

The source terms for equations 2.1 and 2.2 are computed as:

$$j_{ECh} = -\frac{Q_{Nominal}}{Q_{ref}Vol}i_P \tag{2.21}$$

$$\dot{q}_{ECh} = \frac{i_P V + \int_{l_p+l_s+l_n}^{0} j^{Li}(T_{ref}\frac{\partial U}{\partial T} - Uref)\,dx}{l_p + l_s + l_n} \tag{2.22}$$

where i_P is the transverse current density

$$i_P = \int_0^{l_p} j^{Li}\,dx \tag{2.23}$$

The P2D model is more computationally expensive than the previous two, but it is also one of the most popular to this day, since it has been researched and tested very extensively.

3. Description of the study

In order to assess the behaviour of each one of the studied models, a series of simulations with different conditions will be run.

First of all, the geometry will be created. Making use of a preexisting file containing a basic SCiB^{TM} battery cell, we will build a module containing two battery cells connected by a busbar. Then, a mesh will be generated and the materials, boundary conditions and battery specifications will be determined.

At that point, the corresponding simulations will be run: first, a round of simple discharge processes at various C-rates and next, a compound cycle of charge/discharge. The approach to each one of these procedures will be described now.

3.1 Simple discharge response

A round of simple discharge processes will be carried out first. For each of the models (NTGK, ECM and P2D), three discharges with different C-rates will be simulated: one at 0.5 C, another one at 1 C and finally one at 5 C.

The C-rate is a measure of the rate at which a battery is charged or discharged, and it is defined as the ratio between the current through the battery and the theoretical current at which the battery would deliver its nominal capacity in one hour [24]. In the case of the TOSHIBA SCiB, the nominal capacity is 23 A·h, meaning that a current of 23 A will correspond to a C-rate of 1 C and will discharge the battery in 1 hour. The C-rate of 0.5 C will correspond to a current of 11.5 A, and 5 C to 46 A. A simple discharge operation presents a constant C-rate along the whole process.

The variables that will be monitored are the following four:

- Temperature: it is a key variable in electric batteries in general and in Li-ion batteries in particular, due to the fact that if the temperature drops, the battery's discharge capacity will be affected, and if it rises excessively, thermal runaway can occur, leading to an explosive decomposition of the cell. Monitoring the temperature is relevant in order to select an adequate thermal management system (TMS) that dampens the shifts in temperature that might appear. In the case of our study, the external walls are submitted to a convection of air.

- Passive zone potential: it is the voltage of the battery, that is the difference in potential between the positive and negative terminals. As general rule, it decreases with the SOC and increases with the temperature.

- State of charge (SOC): it is a measure of the available battery capacity relative to its maximum capacity [24]. It is measured as a percentage or as a proportion. In our case, a SOC of 1 will mean that the battery is fully charged, and 0 will mean that it is fully discharged.

- Heat source: it is the total heat generated by the battery module. A distinction can be made between different sources: electrochemical heat (also called reversible heat) , Joule heat (due to the Joule effect caused by the flow of electrons through the battery, also called irreversible heat) and short-circuit heat. The first one takes

up the heftiest portion of the total amount of heat generated, and the last one will only have a value if a short-circuit state is given, which will not be the case in this study [14].

To be able to analyse the results, they will be presented in graphs as a function of the flow time. For each one of the variables there will be three graphs, corresponding to each one of the C-rates tested (0.5 C, 1 C and 5 C). In each of the graphs there will be three curves, corresponding to the three models (NTGK, ECM and P2D). With this layout, we will be able to compare the variable response to equivalent processes (with the same C-rate) simulated with each one of the models.

3.2 Compound cycle response

As the second part of our study, the behaviour of each model in the presence of abrupt changes in electrical load will be evaluated. To do so, a compound cycle consisting of several alternated charge/discharge processes will be simulated, with the idea of roughly emulating the performance of a battery in an electric or hybrid vehicle followed by a steady charging process.

The cycle, programmed as a function of the flow time, employs C-rates, current intensities and powers as measures to determine charge and discharge rates. With a total of 1000 seconds of simulation, it is divided in 9 segments:

1. Discharge at 300 W for 150 s
2. Charge at 1 C for 30 s
3. Discharge at 1 C for 60 s
4. Charge at 6 A for 60 s
5. Discharge at 5 C for 30 s
6. Discharge at 0.5 C for 200 s
7. Discharge at 100 W for 60 s
8. Discharge at 400 W for 10 s
9. Charge at 1 C for 400 s

For the analysis of the results, they will be presented in graphs, one for each variable (temperature, voltage, SOC and heat) as a function of the flow time. In each one of the graphs, there will be three curves, corresponding to the response obtained with the three models (NTGK, ECM and P2D).

3.3 Effect of the model parameters

For all the models that have been employed in this study, a series of parameters need to be defined so that the equations that govern the simulation may be computed.

In the case of the NTGK model, the coefficients a_n, b_n and the temperature corrections C_1 and C_2 need to be determined to calculate the parameters U and Y as exposed in

Equations 2.5 and 2.6. The total count of coefficients to determine is 14, since a_n and b_n are a series of six terms each.

For the ECM model, the values for the resistances, capacitances and the open circuit voltage can be defined with several methods, in which there is the need to determine the coefficients of the Sets of equations 2.9 and 2.10, or to define a table with its values as a function of SOC and temperature.

The P2D model has the most amount of parameters to define, such as the thickness of electrodes and separator, particle diameters, number of grids or maximum Li+ concentrations; a total of 49 parameters that are employed throughout Equations 2.7 to 2.23 and make for the most intricate one of the three models.

Due to the lack of experimental data concerning the characterisation of the SCiB^{TM} battery, the results of the previous sections have been obtained retaining the values for the above mentioned parameters that ANSYS Fluent carries by default. Nevertheless, in a confidential report provided by CMT-Motores Térmicos at the Universitat Politècnica de València, a task of "battery cell characterisation, parameter identification and second order equivalent circuit modeling of the battery cell" is carried out. In said paper, the values for resistances, capacitances and open circuit voltage are given as a function of SOC and temperature, and they can be introduced in Fluent as a table.

In order to evaluate the impact of choosing parameters for each model that are in accordance with the specific type of battery that is being studied, the results of the equivalent circuit model with the default parameters and the identified ones will be compared for each one of the studied C-rates and variables.

4. Setup with ANSYS Fluent

4.1 Geometry

The geometry that we will work on, as can be seen in Figure 4.1, is a module formed by two SCiB^{TM} battery cells, separated 1 mm of each other and connected in series by a busbar of 1 mm thickness. To create it, we will use the ANSYS DesignModeler tool.

Starting with a preexisting file containing a single battery cell, we will import it to DesignModeler and duplicate it at the desired position. Now that the two cells are arranged, the busbar will be created by sketching a rectangle and extruding it until it takes up the two connected tabs.

In this first section, one key aspect is to set the different parts and relevant surfaces of the battery as named selections, so that later in the setup step it is possible to assign particular characteristics (materials, boundary conditions, etc.) to each one of them. According to the selections seen in Figure 4.1, we will name 7 parts (2 cells, 4 tab zones and 1 busbar) and 2 surfaces (positive and negative tabs). It is important to notice that the busbar connects cell1 and cell2 through tab zones of different sign.

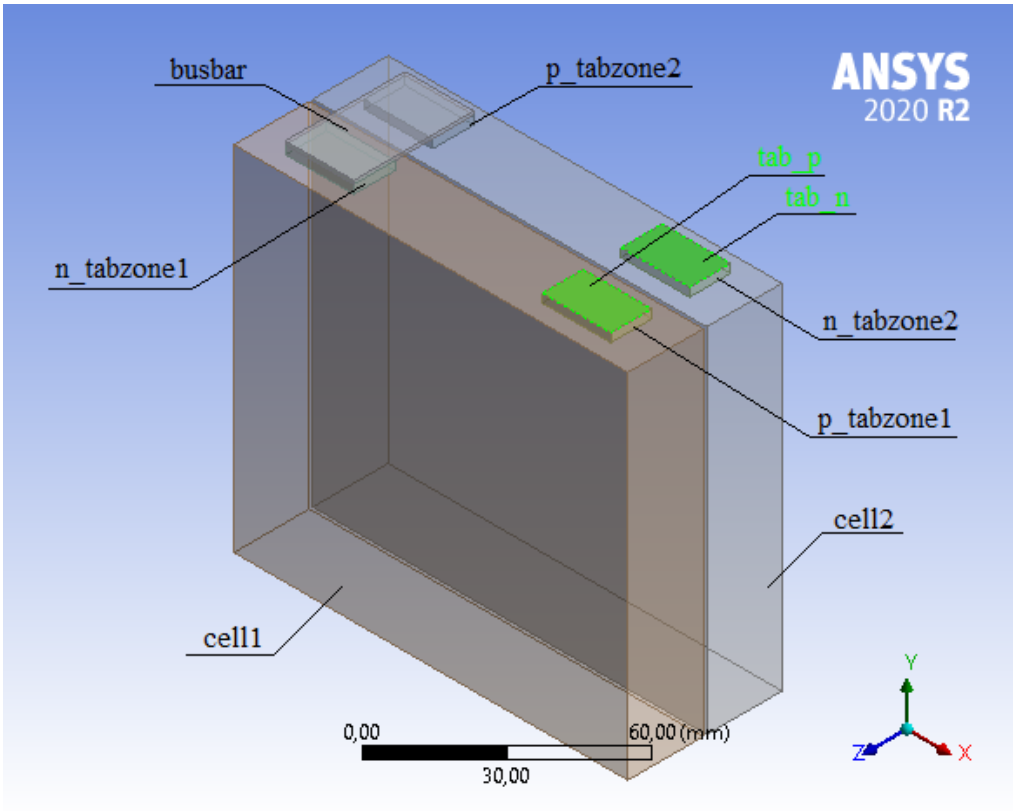

Figure 4.1: Geometry of the battery module with named selections

4.2 Mesh

The Meshing tool of ANSYS will be used to mesh our domain.

To do it, two different sizing settings will be used: the first one, spanning through the tab zones and busbar, will have an element size of 1 mm; and the second one, taking up cell 1 and cell 2, with an element size of 2.5 mm. The reason for this is that, since the tabs are the regions where the current is collected, there is the need to have a higher concentration of cells in them. The elements of the tab zones and busbar have a hexahedral shape, while the ones in the cell are tetrahedral.

The total number of elements is 309643, and a representation of the mesh can be seen in Figure 4.2.

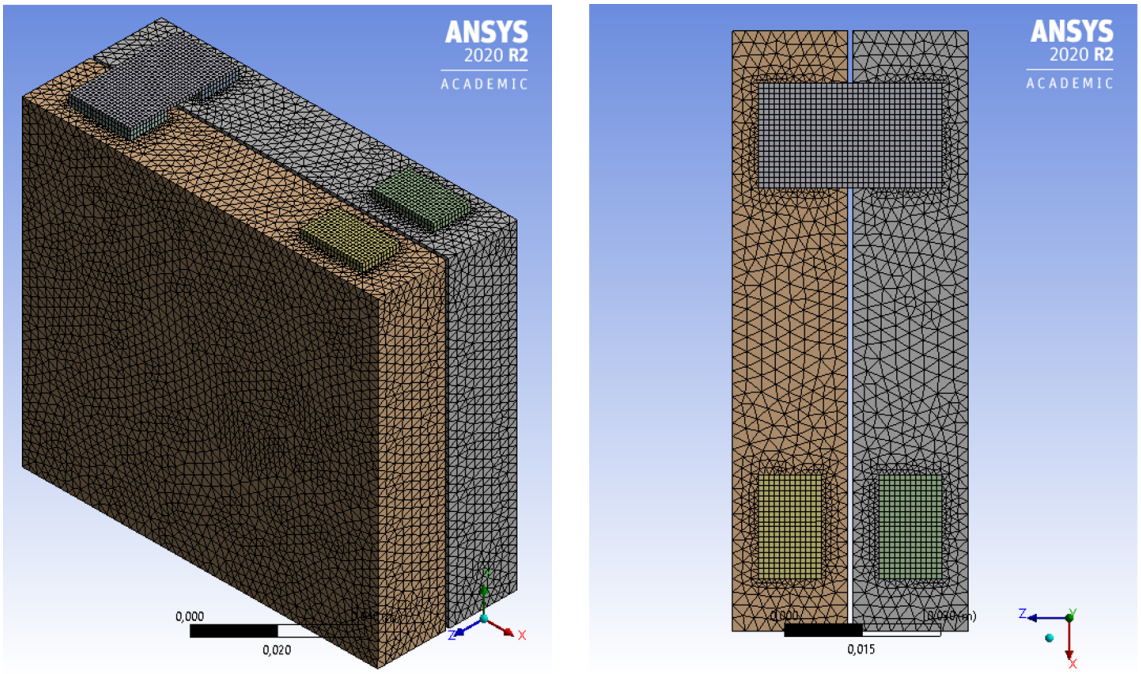

Figure 4.2: Representation of the mesh in (a) isometric and (b) top view

A mesh independence study will not be carried out. The reason for it is that the mesh given by default by the meshing tool (Figure 4.3) has been improved significantly, from 9354 elements to the present count, and given that the version of ANSYS that is being used is an academic one, it is not permitted to work with fluent with a mesh that contains more than 512000 elements. Therefore, an attempt has been made to maximise the element count bearing in mind the limitation of the academic license, and making the consideration that the calculation time used by the simulation is not excessively high for the present amount of elements, it has been deemed more efficient to skip this part of the study.

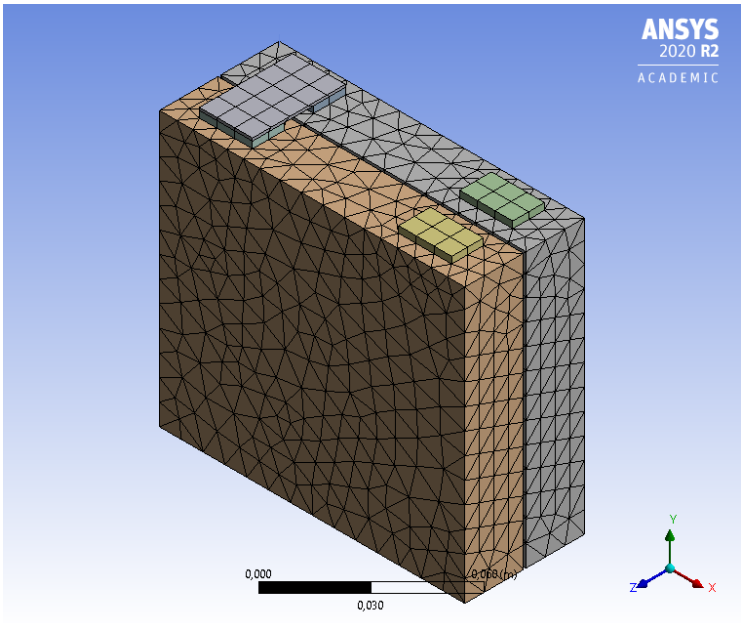

Figure 4.3: Default mesh given by the ANSYS Meshing tool

4.3 Setup

Now, once the mesh is done and loaded into FLUENT, it is time to give the desired conditions to our model. This will be done following the instructions of the ANSYS Fluent Tutorial Guide [3], which can be consulted for a step-by-step explanation, as only a general outline will be presented in this study.

4.3.1. Simple discharge

The first thing is to load the Dual-Potential MSMD battery model add-on, and after enabling the transient state and the energy equation, we will start defining the battery model options.

Here, we can select the method (MSMD) and the model we want to use (NTGK, ECM, P2D or a user-defined one). As it was mentioned in section 3.3, the parameters for this first part of the study will be left as they are by default, and their values are shown in Figure 4.4.

Regardless of the model that we are working with, some aspects of the battery model have to be defined. The nominal cell capacity will be set to 23 Ah, the Joule heat in active zones will be enabled and the C-rate will be specified. This C-rate will be constant along the simulation, which is the behaviour needed for this simple discharge process.

As for the conductive zones, we will define the cells (cell1 and cell2) as active components and the rest of zones (busbar and all the tab zones) as passive. The tabs will be defined as electric contacts: tab_n as the negative tab and tab_p as the positive one.

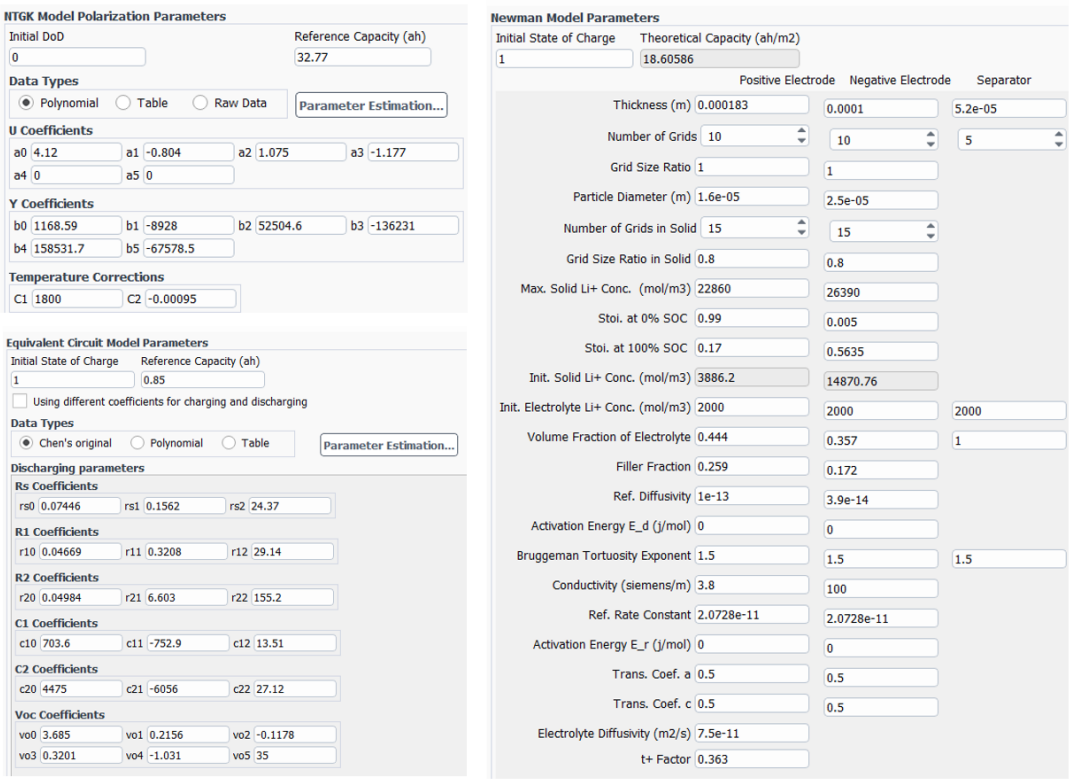

Figure 4.4: Default parameters for the three employed models

At this point, the battery model is fully defined and now the materials will be covered. For our simulation we will use two different materials:

- e_material: it is a solid that will be used for the cells. These are its properties:
  - Density: 2719 kg/m^3
  - Specific heat (Cp): 871 J/kg·K
  - Thermal conductivity: 20 W/m·K
  - Electrical conductivity: 1.0 e6 siemens/m for both user-defined scalars (defined-per-uds)
- bus_material: it is also a solid used for the busbar and the tab zones. It presents the same properties as the e_material, except for the electrical conductivity which is set to a constant of 3.541 e7 siemens/m.

After the materials, the boundary conditions will be established. A thermal condition of convection will be applied to all the walls except for the tabs (tab_n and tab_p, which present no heat exchange), with a heat transfer coefficient of 5 W/m^2K and a free stream temperature of 300 K.

Finally, the last step before the simulation will be to specify the solution settings. The equations of flow and turbulence will be disabled, since there is no fluid flow to be calculated, and the convergence criteria regarding the residuals will also be deactivated. The report definitions that will be created in order to extract information for a future analysis are the following:

- Temperature: volume report of Max Static Temperature for the whole domain.

- Voltage: surface report of Area-Weighted Average Passive Zone Potential for the positive tab (tab_p).
- SOC: volume report of Max State of Charge (SOC) for cell1 and cell2.
- Total heat: volume report of Volume Integral of Total Heat Source for cell1 and cell2.
- Electrochemical heat: volume report of Volume Integral of Echem Heat Source for cell1 and cell2.
- Joule heat: volume report of Volume Integral of Joule Heat Source for cell1 and cell2.

The time step size that has been chosen is 20 s, and the number of time steps will be 100, that is to say, the total flow time will be 2000 s. This applies to all the simple discharge processes, that is to say, to all the models and C-rates.

4.3.2. Compound cycle

In order to input our compound cycle, it will have to be described in a .txt file. In Fluent, two types of profiles can be used: time-scheduled, in which the value of the electric load changes as a function of the flow time, and event-scheduled, in which there is a forwarding condition to change from one load to the next. The distinguishing factor is the number of columns that the .txt file has: 3 for the time-based and 4 for the event-based [6].

The three columns that form the time-based profile are the following:

1. Time
2. Electric load value
3. Electric load type (defined by an integer number)
    - 0: C-rate
    - 1: Current
    - 2: Voltage
    - 3: Power
    - 4: External electric resistance

Therefore, to translate the time profile described in Section 3.2, the .txt file that has to be built as shown in Table 4.1:

To load it into Fluent, the solution option has to be changed from Specified C-rate to Using Profile, and then selected in Specify profile file.

4.3.3. Determination of ECM parameters

The information of the ECM parameters of the SCiB^{TM} has been provided internally by the CMT in the form of graphs. Each one of them presents the values of a parameter as a function of SOC, having each graph several curves corresponding to each one of the temperatures for which the information has been extracted, ranging from 273 K to 318 K. There is a total of six graphs, that is three for the resistances (R_s, R_1 and R_2), two for

0	300	3
150	300	3
150.1	-1	0
180	-1	0
180.1	1	0
240	1	0
240.1	-6	1
300	-6	1
300.1	5	0
330	5	0
330.1	0.5	0
530	0.5	0
530.1	100	3
590	100	3
590.1	400	3
600	400	3
600.1	-1	0
1000	-1	0

Table 4.1: Time-scheduled profile as a .txt file

the capacitances (C_1 and C_2) and one for the open circuit voltage (V_{OCV}), following the outline seen in Figure 2.6.

For the extraction of the numerical values from the graphs to be able to introduce them in Fluent, a web plot digitise tool will be used, available at `https://apps.automeris.io/wpd/`. As a result of the digitisation, the information will be laid out in tables with the same format as the graphs: values of the parameters as a function of the SOC with a different file for each temperature. The values can be introduced in Fluent either manually or with a .tab file.

It is also important to mark that the minimum stop voltage, that is to say, the value of passive zone potential to which the simulation will be stopped, is set to 3 V by default. Given that the SCiB^{TM} battery has a nominal voltage of around 2.1 V, it will be necessary to lower that value so that the stopping criteria is adjusted to the battery model. A suitable value could be 1.5 V.

4.4 Presentation of results

The post processing of results for its presentation will be done with the help of MATLAB, working with the .out files that are the product of the simulation and contain the data of the variables studied as a function of the flow time. With MATLAB, that information will be loaded, extracted and plotted in a way that makes its interpretation as straightforward as possible.

5. Presentation of results

In this chapter, the results of the simulations will be presented and commented. It is pertinent to state beforehand that the very extreme values that appear for the studied variables when the simulations reach a state of charge (SOC) of zero in the simple discharge processes have been removed in order to be able to interpret the graphs adequately. These appear due to the numerical nature of the models and have been deemed to be out of the scope of the study of the discharge processes themselves.

5.1 Simple discharge

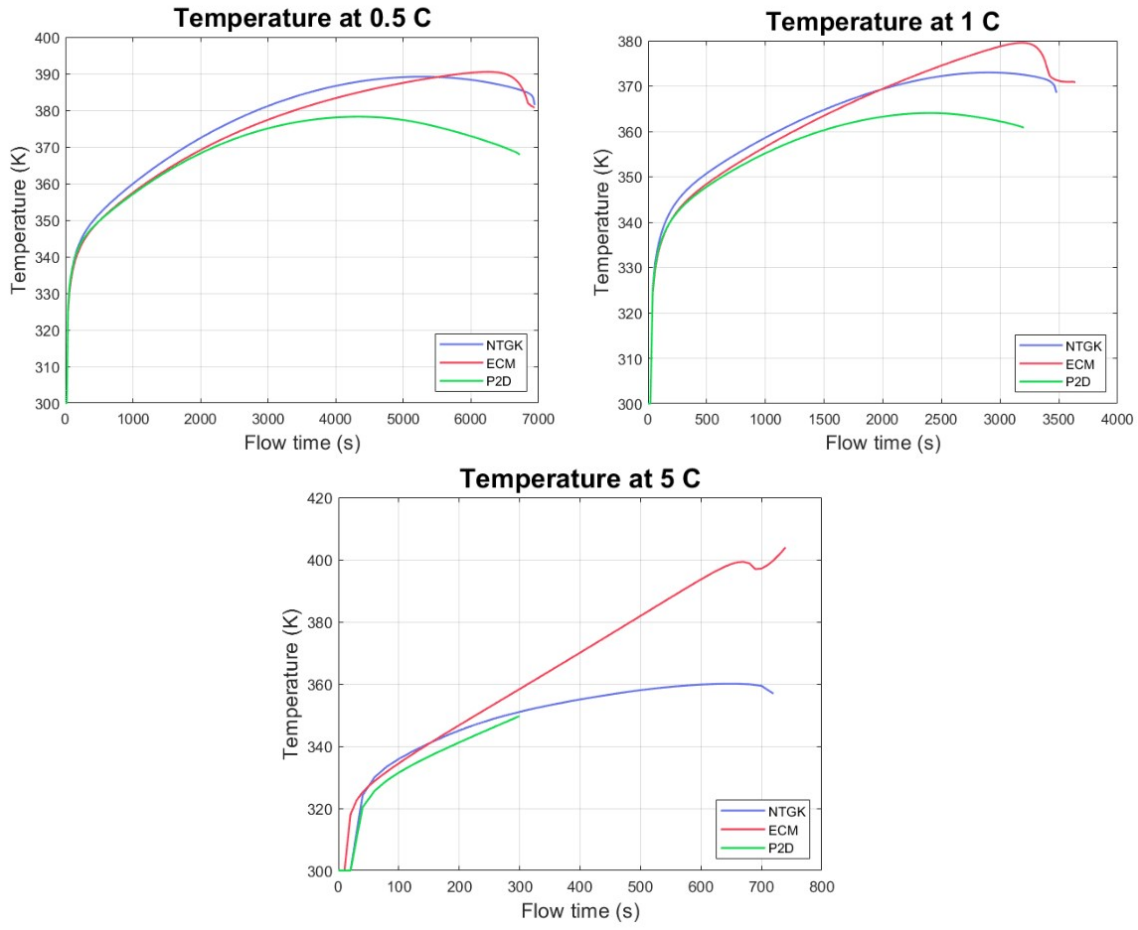

Figure 5.1: Temperature response of each model for different C-rates

The temperature response for the simple discharge cases is shown in Figure 5.1. It can be appreciated that there is a noticeable similarity between the 0.5 C and 1 C profiles, while the 5 C case looks less alike. Also for the two first cases the deviation in the response of the different models is less significant than in the last case.

All three temperature profiles present the same basic behaviour: a steep rise from the initial value of 300 K in the first seconds of simulation followed by a slower, almost

constant increase until reaching the peak point, after which there is a steady decrease, slightly more abrupt in the case of the ECM.

The highest temperature, around 400 K, is reached towards the end of the simulation at 5 C. This is expected, since at high C-rates the current through the battery is higher, leading to a greater generation of heat. Also in the 0.5 C simulation a high temperature of 390 K is reached, probably due to the fact that this case takes up a higher flow time, and therefore the heat generation is accumulated.

The decrease of temperature after the peak could be due to the fact that, as we will study later, the total heat presents a general tendency to decrease with the SOC, and taking into account that there is a convection of cooler air around the battery pack, the heat generated could be being dissipated more easily.

As for the differences between the models, it has already been commented that they seem to increase with the C-rate. This is expected, since the approximations that these models provide are less reliable when the variables take big values. The NTGK model gives the highest initial rise, being later surpassed by the ECM during the course of the simulation, whose peak value is the highest. This is made even more evident in the 5 C case, where the ECM surpasses the NTGK and they go on to reach very different end values, the one for the ECM being much higher.

The P2D model generally gives the lowest values of the three, and the peak value and the temperature descent come much earlier than in the other models. Furthermore, the simulations with P2D are the first ones to stop due to the variables reaching values much higher than those set as stopping criteria (5000 K for temperature), which could be indicative of its greater instability. This is also made very evident in the 5 C case, where the simulation does not even reach half the flow time than the ones with the other models.

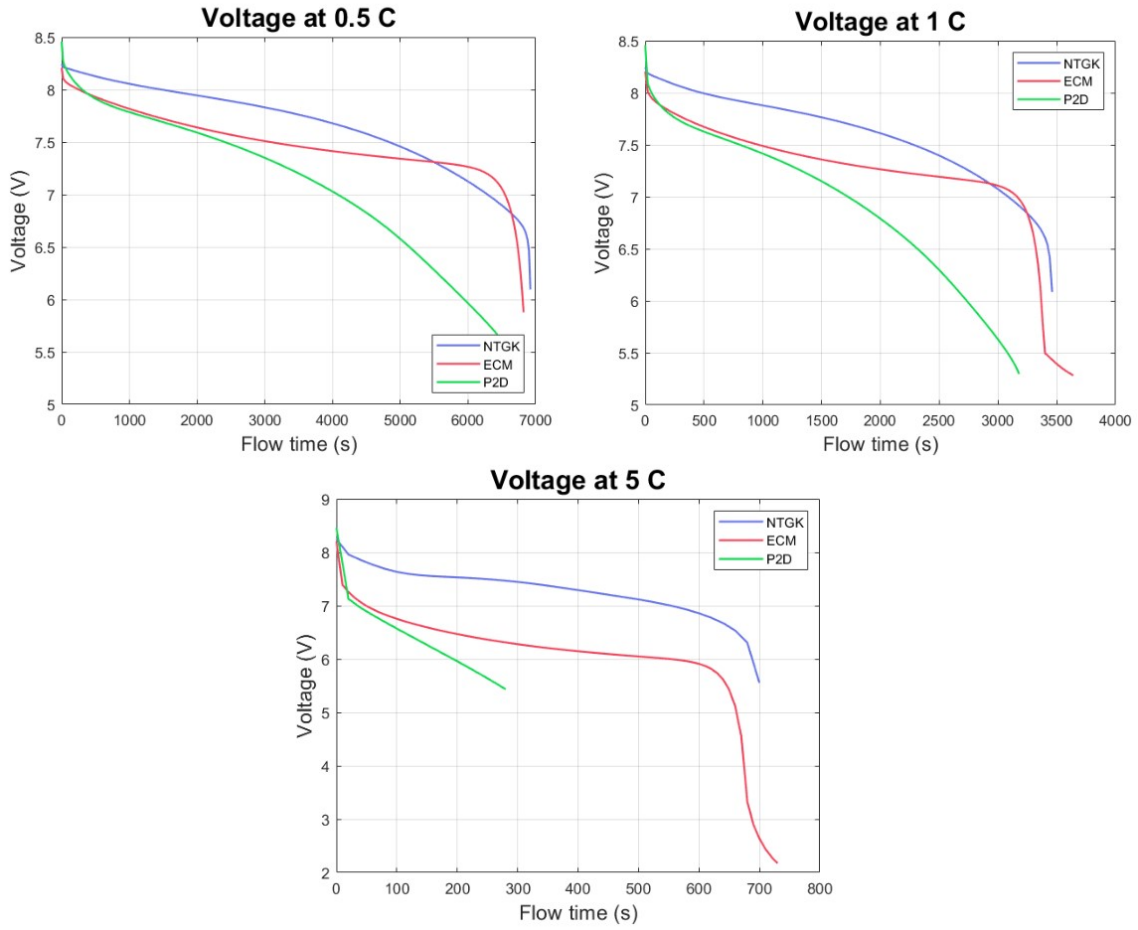

Figure 5.2: Voltage response of each model for different C-rates

In the case of the voltage response, shown in Figure 5.2, the similarity between the 0.5 C and 1 C cases is, again, very notable, whereas the 5 C case has a slightly different behaviour. The curves present almost an inverse trend to that observed in the temperature: an initial drop from the starting value of approximately 8.4 V and then a more steady decrease. Here the two distinct states are commonly referred to as exponential and nominal zones, respectively. At the end of the simulation there is a large drop corresponding to the behaviour of the battery when it is close to being fully out of charge.

In the exponential zone, the biggest voltage drop in the first seconds of simulation corresponds to both the ECM and P2D model, the two of which present a fairly similar behaviour in the early stages of the simulation even if the drop of the ECM occurs faster and the P2D's is a little bit more paced. The NTGK model, as happened with temperature, gives the highest voltage values for the most part of the nominal zone, being then surpassed by the ECM in the two first cases (0.5 C and 1 C). In this nominal zone, the ECM model presents a very small slope, meaning that the voltage does not suffer a big variation during this stage. On the other hand, the slope of the P2D model is the most pronounced of the three, resulting in the most dissimilar values towards the end of the simulation. The slope of the NTGK model has a middle value, even though it bears more resemblance to that of the P2D. The slopes become more steep with an increasing C-rate, meaning that the voltage drop in the nominal zone becomes faster in time.

Furthermore, it can also be stated that the numerical difference in the results increases when the C-rate is high: the difference between the NTGK and ECM model in the middle

of the nominal zone is of roughly 0.25 V for the 0.5 C case, and it grows to up to 0.5 V for 1 C and to more than 1 V for the 5 C case.

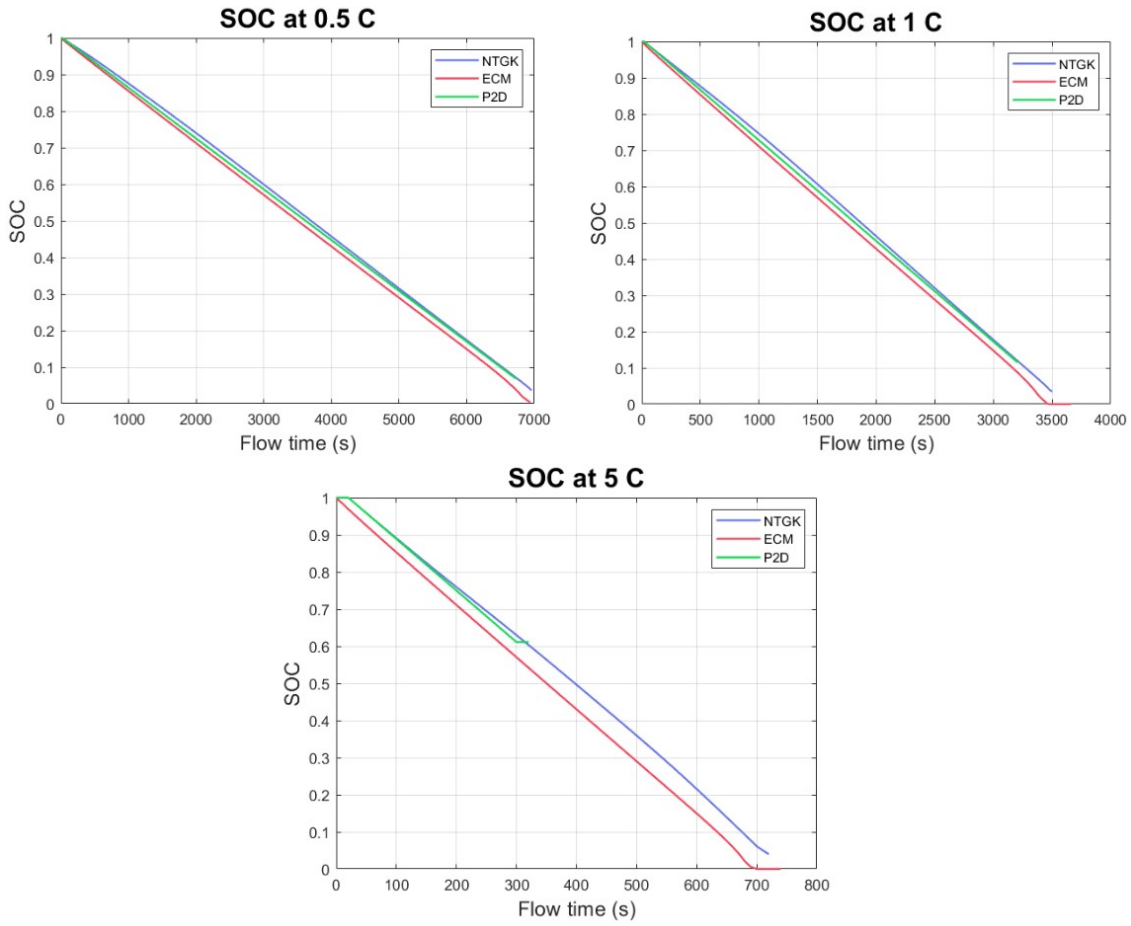

Figure 5.3: State of charge of each model for different C-rates

The state of charge (SOC) presents in Figure 5.3, for all three C-rates and models, an almost perfectly linear decrease from the initial state of 1 until the simulation is stopped. The simulation time of each case has been selected so that the graphs could show the information of the whole discharge process; that is why the majority of them, with the exception of the P2D at 5 C, which reaches a halt while the battery is still not fully discharged, go from a SOC of 1 until a value close to zero.

As it has already been commented, the discharge processes cause a linear descent of the state of charge. The results for each of the models are fairly similar, with a maximum difference of 3% at 0.5 C, 4% at 1 C and 7% at 5 C, which once again makes evident that the discrepancy in the results of each model is stronger when the C-rate is high. Even if the numerical values are close, it can be distinguished that the NTGK model gives once again the highest values and the ECM, the lowest. This is mainly due not only to the slight difference in slopes (less pronounced for the NTGK and steeper for the ECM), but to a delay of 20 seconds (one time step) in the starting of the decrease of the SOC for both the NTGK and P2D models, which can be clearly appreciated in the early seconds of simulation in the graph for 5 C.

The most noticeable aspect of these plots is the stopping point of the simulations, in particular for the P2D model. Already in the 0.5 C case, it can be noted how it stops earlier than the other two models, reaching a final SOC of 0.06. At 1 C, it stops at a 0.12 SOC, and at 0.61 for 5 C, amounting to even less than half of the flow time that was

expected and that the other models did reach. This fact could be indicative, as was already mentioned in the beginning of this section, of a numerical instability of the P2D model, which could be linked to the fact that it is also the most computationally demanding of the three.

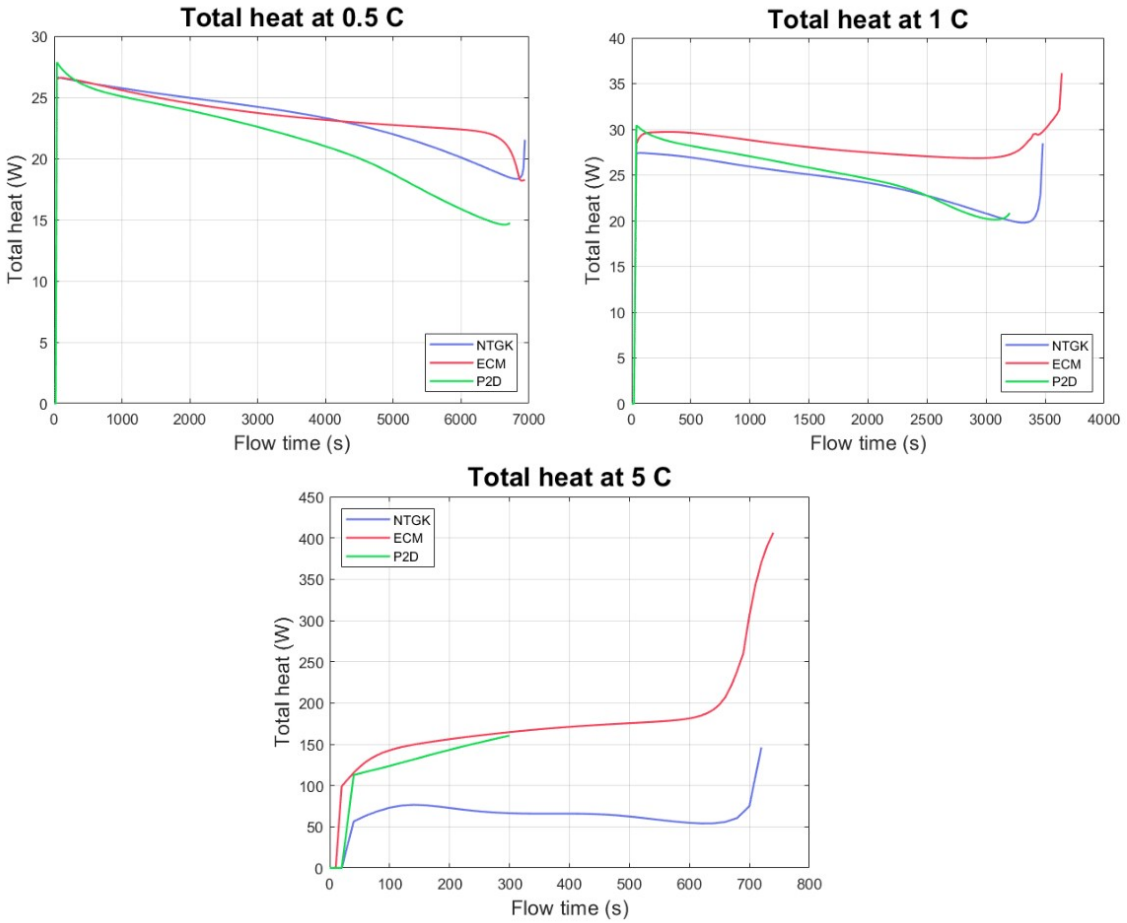

Figure 5.4: Total heat of each model for different C-rates

The analysis of the total heat (Figure 5.4) is closely related to that of the temperature, already carried out in the beginning of this section. The behaviour follows the same pattern that has been observed so far: an exponential zone first, where the generation of heat grows a lot in a short time, and a nominal zone where the evolution is more steady. The magnitude of the peak of the exponential zone grows with the C-rate, and regarding the nominal zone, a general decreasing tendency is shown, even though this is not the case for the case at 5 C in the ECM model.

In most curves, a sudden rise takes place at the end. It could be due, as it has already been commented, to the numerical nature of the models, which give out unreliable results that do not resemble the actual behaviour of a battery when the state of charge approaches zero. This is the cause for the stopping in the simulation: since the total heat generation is triggered, so is the temperature of the cell, and these high values that exceed the stopping criteria bring the simulation to an end. This activity could also be indicative of a thermal runaway process, but the fact that it takes place only at low states of charge and that in most cases the sudden rise comes after a steady decrease in heat generation makes this possibility seem unlikely.

As for the differences between models, here the pattern of behaviour does not come through as clearly as it appeared in the rest of variables. Some particularities that can

be seen are that the initial peak of the P2D model is sharper than the others, and that the ECM model gives the highest results in the two cases with highest C-rate. This last aspect can be appreciated at 5 C in the temperature response (Figure 5.1), where the ECM shows considerably higher values than the NTGK.

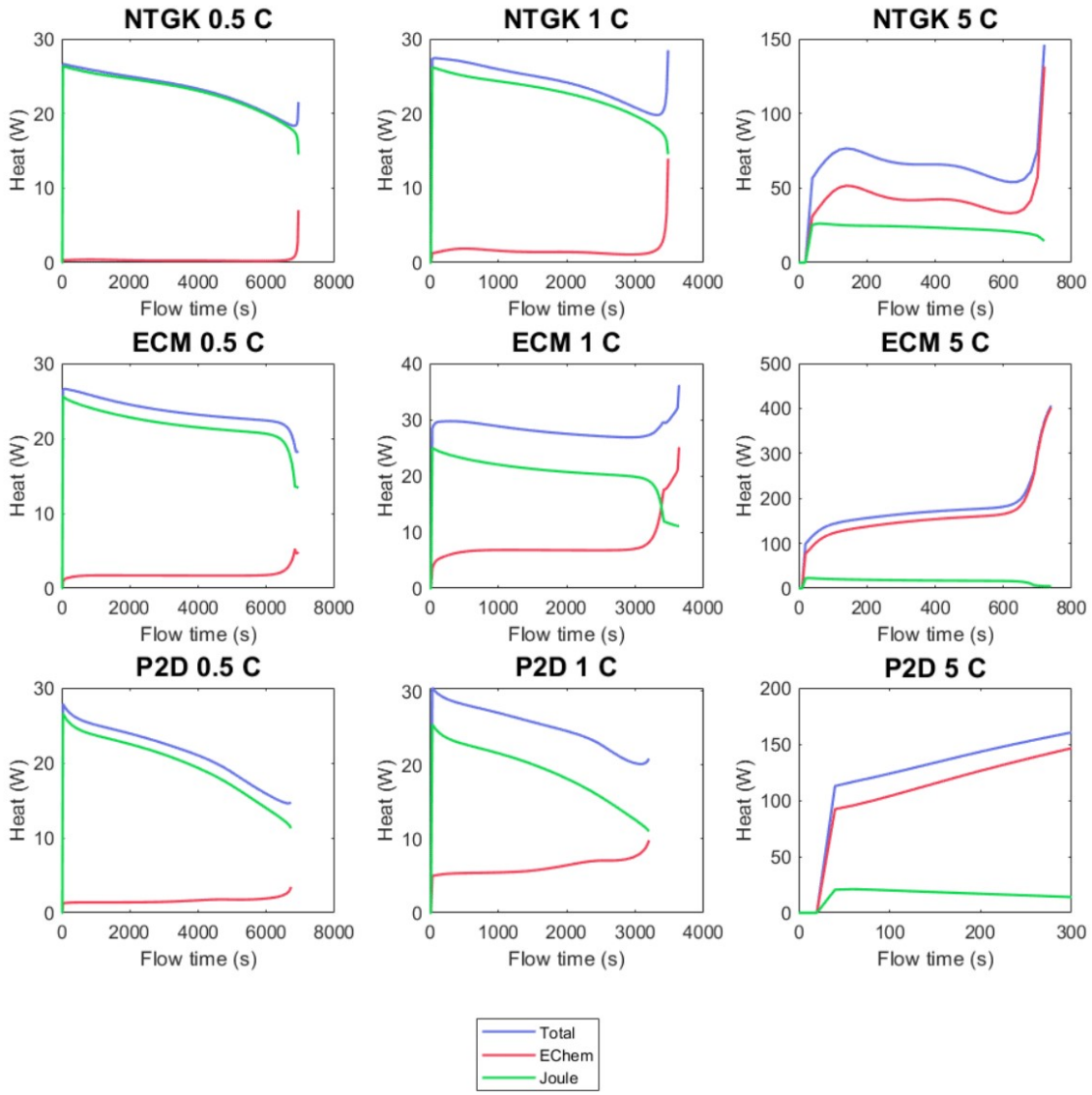

Figure 5.5: Comparison of total, electrochemical and Joule heats of each model for different C-rates

In Figure 5.5 the total heat has been broken down into reversible (electrochemical) and irreversible (Joule) heat.

It stands out very clearly that the influence of the C-rate in the proportion of each one of the heats is significant. At low C-rates (0.5 C), the Joule heat has a strong predominance over the electrochemical, which takes very low values in comparison. At 1 C, this proportion is not as biased but the Joule heat still contributes a strong part of the total heat, and at high C-rates (5 C) the ratio is flipped, and the Joule heat becomes minor against the electrochemical. Consequently, it can be extracted that, while Joule heat remains roughly constant with the C-rate, the electrochemical heat generation becomes higher with it.

This analysis can be seen in the results of all three models. However, there are particularities that can be detected. For example, it is notable that in the NTGK model the values for the electrochemical heat are considerably lower than in the other two for all C-rates, while there are no obvious differences in the values of the Joule heat. In the ECM, the Joule heat is more constant throughout the discharge than in the other models, where it varies more steadily and the curve shows a steeper slope in the nominal zone. Finally, in the P2D model, the distinct characteristic is that at the end of the curves there is not a sudden variation in the heat values, in the other cases the electrochemical and Joule heat suffer an abrupt increase and decrease, respectively. This is linked to the already commented fact that this model is the one whose simulation comes to an end the earliest, not giving a chance for this end behaviour to take place.

5.2 Compound cycle

In Figure 5.6 the responses to the compound cycle described in Section 3.2 are shown. To get a sense of the evolution of the cycle, the graph of the SOC can be consulted, since it is the most representative because it shows the rates at which each segment of the cycle charges or discharges the battery. In the following lines, each graph will be analysed.

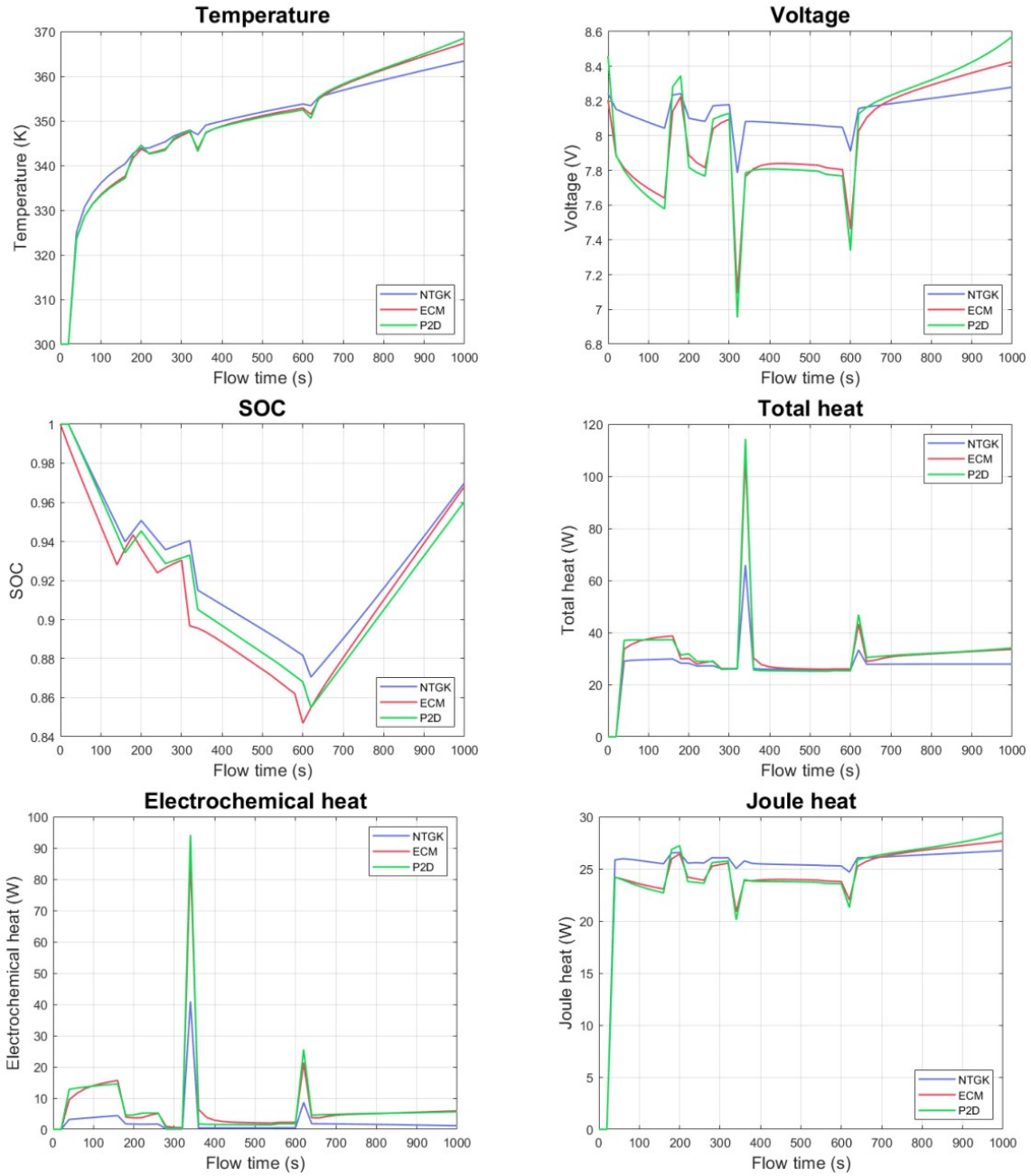

Figure 5.6: Response of the variables to a compound cycle for each model

Overall, the most noticeable and significant aspect of this model comparison is that the results of the NTGK model differ visibly from the results that the other two models give, which are numerically closer. This is due to the fact that, as was mentioned in Section 2.3.1, the NTGK model does not account for inertial changes in the face of sudden surges in the electrical load [5], and therefore its performance with this compound cycle is not optimal. However, even if the ECM and P2D model are more consistent, a noticeable

difference is also made apparent: for a shift in electrical load, the studied variables suffer higher variations in their values with the P2D model, which takes slightly more extreme values, while the behaviour of the ECM is more buffered, and the changes are less sharp.

Many traits that stood out in the responses to the simple discharge processes are observable here, too:

In the temperature, the strong initial rise of the NTGK model is something that happened already in Figure 5.1, as well as the lower values at the end. It is interesting to watch the decreases in temperature around t = 200, 320 and 600 s. These seem to take place when there is a discharge of the battery following a process with a lower C-rate or a charge segment.

In the voltage, the high values at the beginning and low at the end characteristic of the NTGK are seen again. This is the best example of how the ECM, in comparison to the P2D, presents smoother jumps when the electrical load shifts are applied. The values for the voltage vary between 7 and 8.6, approximately. Exponential and nominal zones appear every time that the electrical load changes, even if it is at a smaller scale or the nominal zone does not have time to appear because a segment is too short in time. When there is a charging segment, or when there is an electrical load that is less demanding than that of the previous segment, the voltage experiences an increase, a behaviour that we did not have the chance to observe in the simple discharge processes. The two biggest voltage drops, around t = 320 s and t = 600 s, correspond to the two segments at highest C-rate and power.

The graph of the SOC is very useful to see what the effect of each segment is on the battery, since each one of them is very clearly defined by a certain slope. The more negative the slope, the more demanding the applied electrical load is, and on the contrary, the higher the charging rate is, the more positive the slope of the segment will be. In consequence, the sections with the most negative slope, which are a discharge at 5 C between t = 300 s and t = 330 s and a discharge at 400 W between t = 590 s and t = 600 s, correspond to the two distinctive peaks that most stand out in the rest of the graphs (the drops in temperature and voltage and the peaks of the heat). As for the performance of the models, the tendency here is very similar to that shown in Figure 5.3, where the ntgk gives out the highest values, followed by the P2D and ending with the ECM, with the lowest values. Another similarity is the 20 second (one time step) delay in the responses of NTGK and P2D models, which is carried on throughout the entire cycle, being observable that the reaction of these models to the electrical load shifts is lagged with respect with that of the ECM. An aspect that was not evidenced in the simple discharge processes is the behaviour of the ECM during the charge segments. Here it is easy to see that the rate of charge, graphically represented by the slope of the line, is higher than that of the other two models, which are practically parallel. This means that the slope of the ECM line is more positive than the others, a trait that can be checked at the second, fourth and last segments of the graph, which represent charging processes.

As for the total heat, the highest peaks appear when high electrical loads are applied, in the fifth and eighth segments. However, a certain delay is made apparent. If the response to the eighth segment is analysed, which consists of a discharge from t = 590 s until t = 600 s, it can be seen how the rise in heat generation starts roughly 10 seconds after the beginning of the segment, and the whole peak is characterised by that delay. Regarding the behaviour of the models, the NTGK presents the lowest values, giving the impression of being buffered or dampened with respect to the others. In the electrical load shifts, when the values of heat also present abrupt changes, it can be seen how the transitions of the ECM model are smoother, while the P2D's are more severe. It can be seen in the graph where there are sudden changes in the slope: the first model presents

smoother readjustments, with rounder shapes, and the second is characterised by more severe angles. The same happens in the peaks, where the values for the P2D are higher than those of the ECM, even if the difference is much less prominent than that of the NTGK's. Finally, it is noticeable that the general decreasing tendency that was observed in the discharges is not observed in this cycle. If anything, it can be said that the opposite is observed for the charging segments, mainly in the last one (from t = 600 s to t = 1000 s), where the tendency is for the heat generation to grow in time, a behaviour that is translated to the rate of growth of the temperature.

In the distinction between electrochemical and Joule heats, the same overall performance of the simple discharge processes is observed: the Joule heat prevails over the electrochemical at low electrical loads, while the reverse happens for high ones, where the electrochemical heat skyrockets and takes over the biggest part of the total heat generation. In fact, while the variation in the values of the Joule heat is not very sizable, some small drops can be seen at the high load segment. The low values of the NTGK model can be observed in the electrochemical heat, but not in the Joule, where its values are actually bigger than the rest, and the difference in the transitions of the ECM and the P2D model can be observed in the graphs of both heats. In general, it could be stated that the behaviour of the electrochemical heat is more present when the behaviour of the total heat is analysed, and more of its characteristics come through, since the Joule heat does not present large variations throughout the cycle.

5.3 Effect of the model parameters in the ECM model

In this section the effect of the model parameters on the results of the simulation of simple discharge processes will be assessed. The determination of the parameters of the battery that is being simulated is key in achieving rigorous results, since the default parameters of the Chen model in ANSYS (they can be consulted in Figure 4.4) are representative of a battery model that might be very different to that which is being studied, and while they provide a base for the study of the Equivalent Circuit Model itself that is being carried out in this paper, they might not be suitable to model specific batteries for further applications. In the next lines, the influence of the modification of the parameters in the studied variables will be commented.

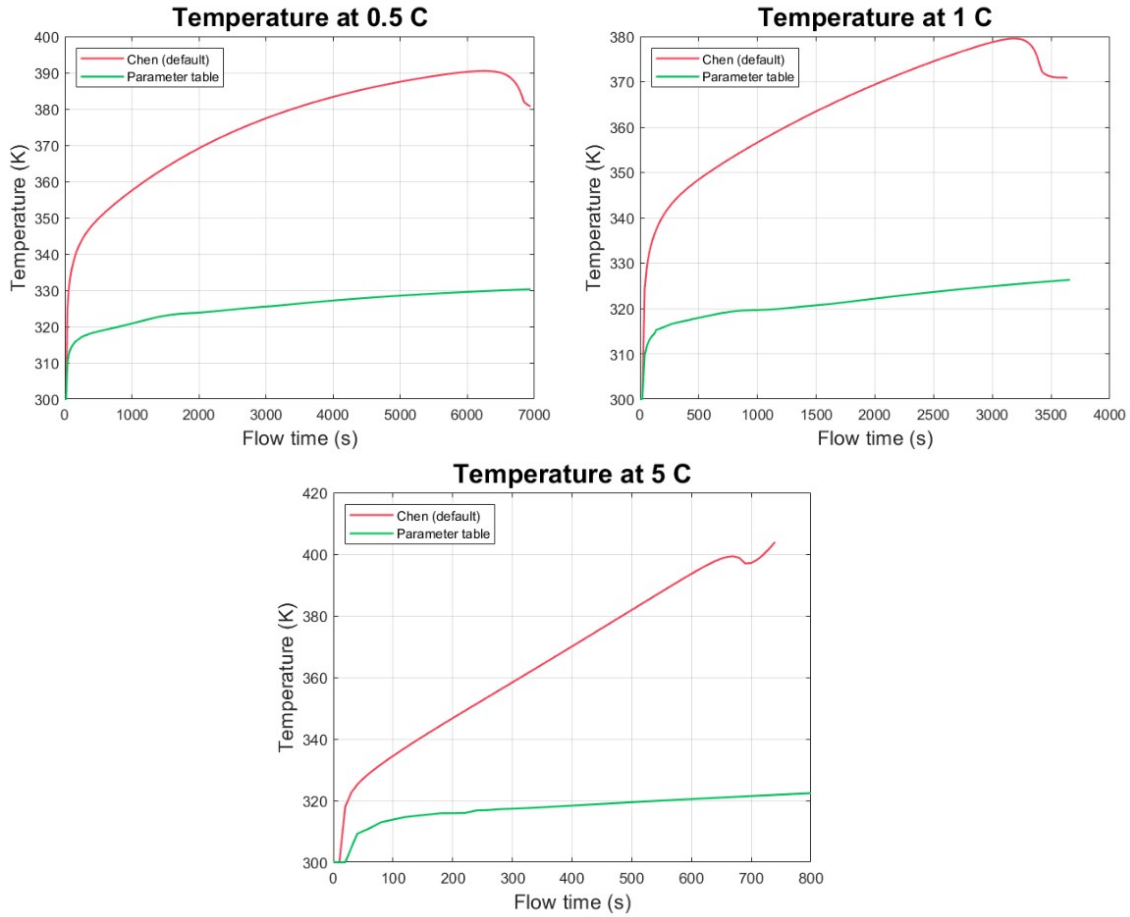

Figure 5.7: Temperature response of the ECM with default and table parameters for different C-rates

Starting with Figure 5.7, it can be seen how the temperature for the table parameters is overall much smaller than that registered for the default Chen case. The initial rise is not as big, only around 15 K in the early stages of the simulation, while in the original case it was of about 50 K. It can also be seen that the temperature growth rate is much slower (smaller slope) and roughly constant (it is a straight line, not a curve). In fact, it can be stated that the behaviour of the temperature is not greatly affected by the C-rate, since for all three cases the initial rise is very similar and so is the rate of growth, being a higher temperature achieved for lower C-rates only because the flow time is bigger.

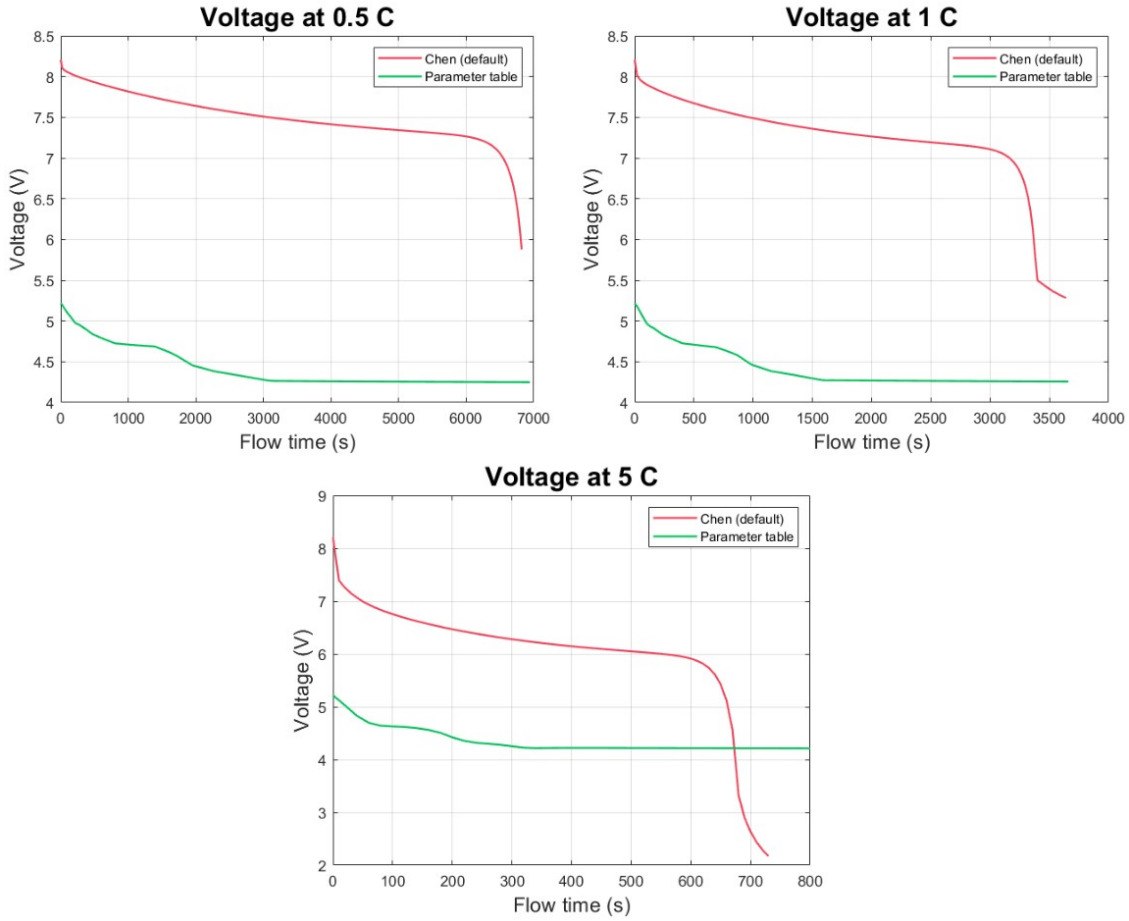

Figure 5.8: Voltage response of the ECM with default and table parameters for different C-rates

The voltage (Figure 5.8) is also overall much smaller than in the Chen default case. We see that the initial voltage of 5.2 V of the parameter table case is considerably lower than the 8.2 V of the original case. Then, the exponential phase is slower and longer, which leaves a shorter nominal phase until the voltage drop, which comes earlier because of the influence of the SOC. However, after this voltage drop when the battery is discharged, the value of the voltage does not remain at zero. Instead it stays at a limit value that, if Equation 2.8 of the ECM is consulted, can be identified as the open circuit voltage, and is in accordance with the data that was given for the parameter table (V_{OCV} for SOC = 0 was around 2.1 V, and since the battery module is built by two cells, the limit value is the double of that). Consequently, the nominal voltage for the parameter table case is lower, too, a value around 4.6 V that is in accordance with the double of the SCiB^{TM} cell nominal voltage, 2.3 V [25]. For the Chen default case this nominal voltage was around 7.5 V.

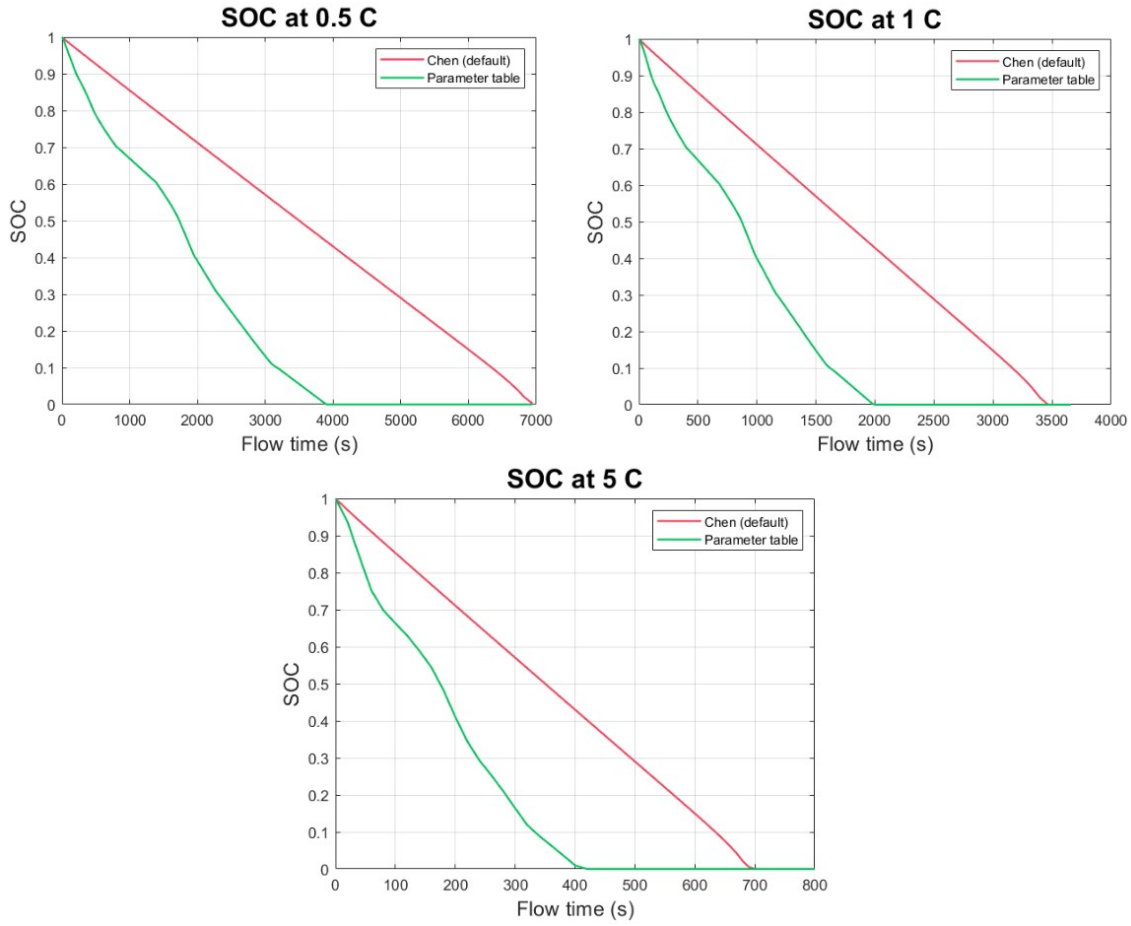

Figure 5.9: State of charge of the ECM with default and table parameters for different C-rates

The evolution of the SOC (Figure 5.9) for the parameter table case is much more irregular and faster than for the Chen default case: the linearity that characterised the original case is not observable here, and the time taken to reach a state of charge of zero is a bit more than half of that taken originally. Furthermore, when the full discharge is achieved, with the Chen default parameters the simulation was triggered and stopped, and outlying values appeared for the variables. That is not the case for the parameter table case, in which the SOC remains at zero and the simulation keeps running, therefore assigning values to the variables by computing the ECM equations. However, the behaviour displayed after the battery is fully discharged is out of the scope of the study of the discharge processes themselves, and will consequently not be object of extensive analysis.

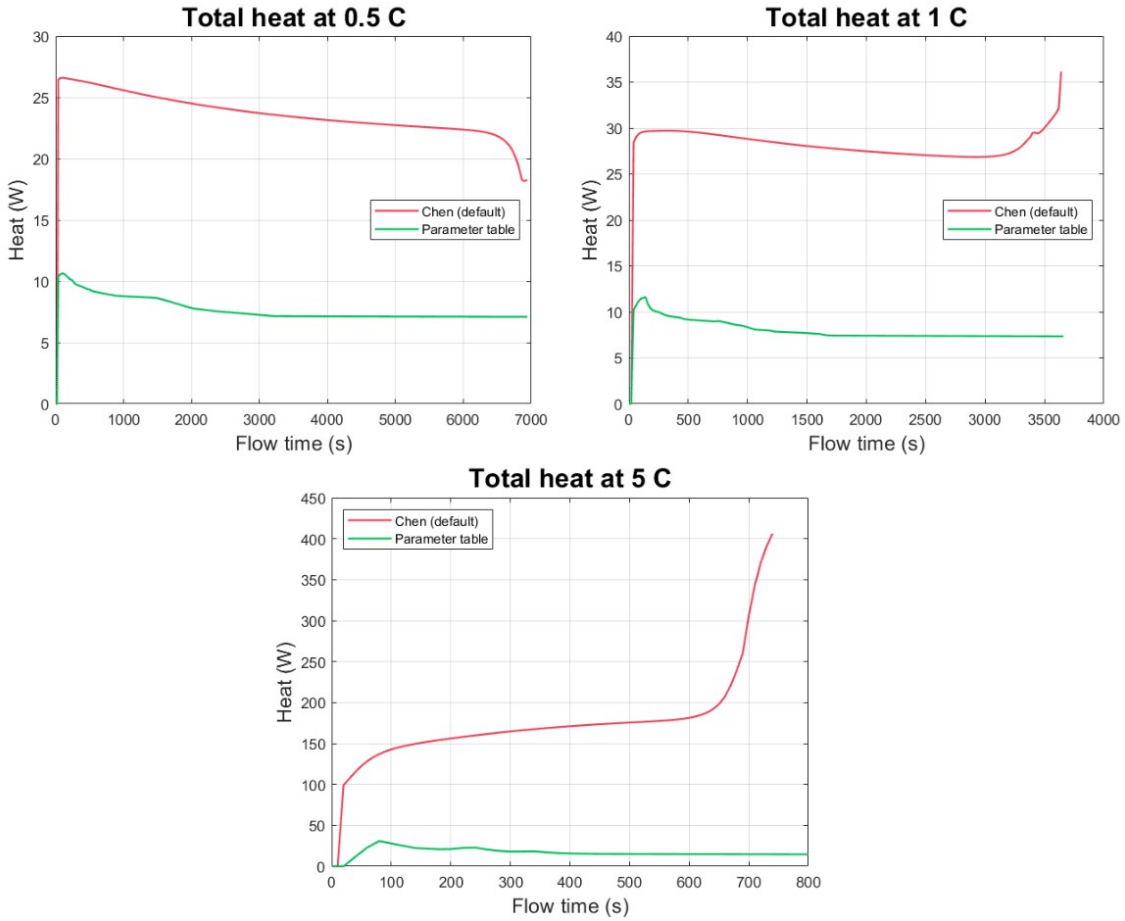

Figure 5.10: Total heat of the ECM with default and table parameters for different C-rates

The total heat (Figure 5.10) is also much lower in the case of the parameter table. It can be noticed how the initial peak is less intense and then the gradual decrease is more irregular. Finally, it stabilises at a certain value and does not vary during the rest of the simulation, a behaviour that was not seen in the simple discharges with the other models. As for the evolution with the C-rate, the increase of the total heat when higher electrical loads are applied is more moderate in the case of the parameter table than for the Chen default case, being the difference in values between these two bigger in the high C-rate case.

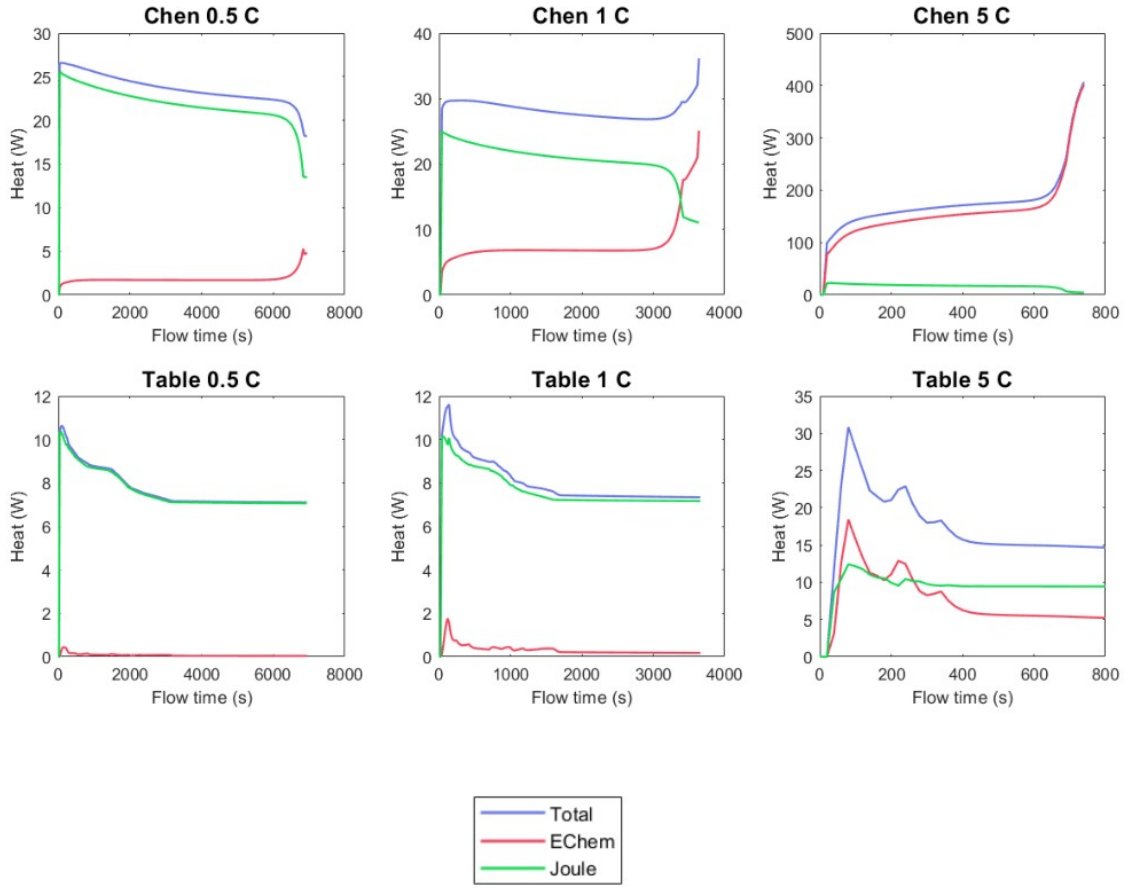

Figure 5.11: Comparison of total, electrochemical and Joule heats of the ECM with default and table parameters for different C-rates

Finally, a comparison of heats (Figure 5.11) in the same format as in Section 5.1 was laid out, where the weight of electrochemical and Joule heat in the total heat generation is analysed. Overall, the predominance of the Joule heat is much stronger for the parameter table, being the case at 0.5 C and 1 C that the electrochemical heat have values very close to zero and the Joule heat constitutes the most part of the total. Also some irregularity can be seen, noticeable in the fact that the lines are not as smooth and continuous as in the Chen default case, a behaviour that is exacerbated in the high C-rate case, where the peaks and valleys are very amplified. This could be due, partly, to the fact that since the total heat in the parameter table case is much smaller, the scale is also reduced, being the roughness in the lines more visible.

6. Comparative analysis of the models

Once the behaviour of the variables has been analysed, the performance of the models itself will be commented and compared, focusing the most attention in the computation cost and the particular trends that have been made evident during the study of all the cases.

6.1 Computation times

	NTGK	ECM (Chen)	P2D	ECM (Table)
0.5 C	11013 s	8658 s	11449 s	16338 s
1 C	6413 s	4280 s	9555 s	7449 s
5 C	1160 s	1324 s	524 s	2744 s
Compound cycle	4250 s	3378 s	3108 s	N.A.

Table 6.1: Computation time, in seconds, of all the studied cases for each one of the models

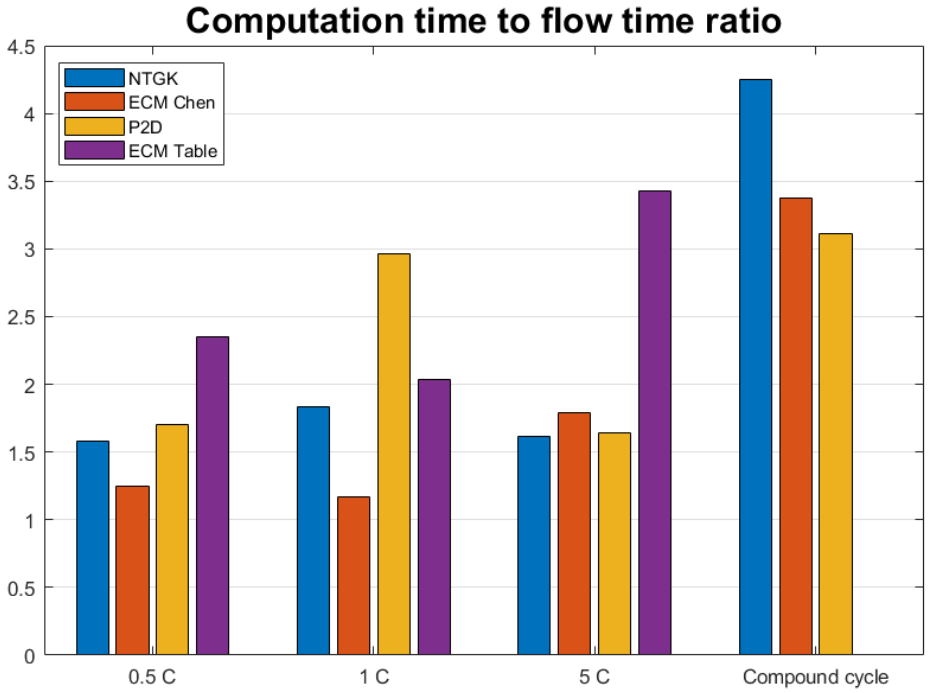

Figure 6.1: Bar graph of the ratio between computation and flow times for each model and electrical load studied

In Table 6.1 the computation time taken by each model in every case can be consulted. To have an idea of what the weighted computational cost of each case is, in Figure 6.1 the

ratio between computation time and flow time of each case and model is given, that is to say, the number of seconds of computation that each second of the simulation requires.

With the NTGK model, it can be seen that its time cost is not affected greatly by the C-rate in the simple discharge processes, but its computation to flow time ratio rises to more than double than that of the previous cases during the compound cycle, indicating that the sudden changes in electrical load are a factor that slows down considerably the rate of computation.

The same happens with the ECM with Chen default parameters, which is in general faster than the rest of the models, even though in the simple discharges a moderate increase in time cost can be observed at a high C-rate (5 C). In the compound cycle, the computational cost increases to a point where it is higher than that of the P2D, but still considerably lower than that of the NTGK.

If ECM was, on average, the fastest of the three initial models (excluding ECM with table parameters), P2D is the slowest one for the simple discharges. At 0.5 C, the difference is not very noticeable, and at 5 C it is even faster than the ECM with Chen default parameters and very similar to the NTGK. It is in the 1 C case where the computational cost is significantly higher than any of the other models, including ECM with table parameters. In the compound cycle, it is the fastest of the three initial models, leading to believe that it is a versatile option that is able to efficiently assimilate the changes in electrical load.

The ECM with table parameters is only applicable to the simple discharge processes, but it is the slowest option by far. Only in the 1 C case it is surpassed by the P2D, but in the rest of the cases its computation cost exceeds significantly that of the three initial models. The difference is more severe in the high C-rate case, where the other models have a similar computation to flow time ratio that is far below that of the ECM with table parameters, which also presents its highest ratio of the three cases. The fact that the computational cost of the ECM differs so much depending on how the parameters are defined is indicative that the introduction of the parameters in the form of a table, even if it allows for a more precise simulation, is very demanding for the computation and slows it down significantly.

6.2 Performance analysis

One general aspect that is very outstanding in the performance of the models in the battery simulation is that as the electrical load (the C-rate in our simple discharge cases) increases, the difference between the results that each of the models gives grows bigger. In the simple discharges, even if the processes at low C-rate last longer (higher flow time), the evolution of the variables according to the different models bear more similarity among each other than that of the high C-rate cases. The reason for this is that, due to the numerical nature of the models, the introduction of high values for the electrical loads in the equations makes the results of the variables differ more from one model to another. The more steady a loading process is, the more cohesive the results are, since the models do not provide optimal responses when extreme scenarios take place. The most severe example of this is a thermal runaway case, in which the simulations' validity cannot be granted because they do not provide tools to cope with the very large values that the variables take.

As for the definition of the parameters, it can be extracted from the study in Section 5.3 that while the analysis of the simulations carried out with the ANSYS default parameters is a tool to examine the behaviour and particularities for each of the models, it is not

suitable for the modelling and study of a specific battery, the reason for it being that the difference between the results of the ECM with the default Chen parameters and the table parameters is very significant, not only in the numerical values of the variables but also in the general trends and characteristics of the simulation. Therefore, even if the geometry employed throughout the study has been that of a TOSHIBA SCiB^{TM}, the results of the simulations that use the default parameters will not be in accordance with the expected ones, since it is also necessary that the specific characteristics of the battery chemistry are accounted for in the introduction of the parameters.

Regarding the comparative analysis of the models, the following can be said about each one of them:

The NTGK model is generally a suitable option to model simple discharges in a battery pack, offering very reasonable results with a medium computational cost. It is only in the distribution of electrochemical and Joule heats that it differs notably with the other models, presenting a tendency to give lower values to the electrochemical heat and higher to the Joule heat. Nevertheless, its performance when dealing with sudden changes in the electrical load is not up to mark, since it is incapable of adapting itself to the cycle, resulting in inaccurate results for the variables, and also its time consumption is significantly higher than that of its counterparts.

The most outstanding characteristic of the ECM is its low computational cost when loaded with the default Chen parameters. That is due to the low amount of equations that are to be solved in each iteration, and their relative simplicity. It is when the parameters of the specific battery are introduced as a table that the simulation time soars and surpasses in most cases those of all the other models. In the compound cycle case, it shows capability of adapting to the load shifts, and its results are very similar to those of the P2D even if they are slightly buffered in comparison. In fact, the similarity can be appreciated already in the simple discharges, where in some cases the initial responses of the ECM and P2D show resemblance.

Finally, the P2D model shows great adaptation to the changes of the compound cycle. Even if it is widely used due to its accuracy, it has generally the highest computation cost of the three originally studied models, and also the most parameters to be defined if a specific battery is to be simulated. However, it did not show a good performance in the high C-rate cases of the simple discharges, since the simulation stopped at an early point and did not reach results that could be compared with those of the other two models.

7. Conclusions

Investigation in the field of electrical power sources can result in an upcoming extensive contribution to the improvement of the environmental situation that global warming poses, with a hefty reduction in the usage of fossil resources and noxious emissions that transportation entails in the present day. The reduction in costs and risks in their implementation is already a reality, made evident by the rising number of HEVs and EVs available in the market.

From the study of the three electrochemical models carried out in this project it can be extracted that each one of them presents peculiarities, making their application suitable and optimal for different scenarios.

For the NTGK model, it has been verified that it is deficient in the presence of compound cycles with load shifts, but it has also been proven that it does not provide the best computation efficiency and that it offers a biased result when observing the comparison of electrochemical and Joule heat sources. Nevertheless, it presents an adequate behaviour in the simple discharges.

As for the ECM model, its simplicity makes for very efficient simulations that were nonetheless slowed down when the default parameters were changed. Moreover, it offers a very satisfactory response when faced with the compound cycle.

The P2D model gives, too, a competent response to the compound cycle, but its time performance and its instability with dealing with high C-rates are among its most considerable weaknesses. Nevertheless, it is a very widely used model that has been researched extensively.

8. Budget

In this chapter, the cost of the present project will be detailed in euros, breaking it down into human resources, equipment, electrical consumption and software costs.

Transportation costs have not been regarded, since due to the COVID-19 pandemic situation the project has been developed telematically.

8.1 Human resources

This part contemplates the retribution received by the participants in the project. That is, in this case, the student or author of this project and two supervisors, both of whom will be considered as lecturers or associate professors at UPV.

For the student's retribution, the monthly payment of an internship at CMT has been considered, which amounts to 400€for a daily work time of 3 h. As for the lecturers, a yearly retribution of 30139.94€has been considered for a total of 1750 hours.

The information of the time dedicated to the project by each part and their hourly retributions is gathered in Table 8.1

	Total time	**Hourly retribution (€/h)**	**Subtotal (€)**
Student	300	6.37	1911
Tutor 1	20	17.22	344.40
Tutor 2	30	17.22	516.60
		Total	**2772**

Table 8.1: Cost associated to human resources

8.2 Equipment costs

The technological equipment employed in the development of the project is an HP OMEN 15 laptop, the total cost of which is 1100€. Nevertheless, if an amortization period of 5 years is taken into account, the cost associated to the duration of the project (8 months) is presented in Table 8.2.

	Cost (€/month)	**Usage period (months)**	**Total (€)**
Laptop	18.33	8	**16.67**

Table 8.2: Cost associated to technological equipment

8.3 Electrical consumption

In this section the electrical consumption of the technological equipment and the conditioning of the workspace will be computed. The consumption of each element will be the following: 0.150 kW for the laptop, 0.015 kW for the lighting and 0.5 kW for heating and conditioning. The cost will be computed over the 300 h of work that have been considered

and the unitary cost will be set to an average of 0.17 €/kW h. The calculations for the electrical costs can be consulted in Table 8.3.

	Consumption (kW h)	Unitary cost (€/kW h)	Subtotal (€)
Laptop	45	0.17	7.65
Lighting	4.5	0.17	0.76
Conditioning	150	0.17	25.50
		Total	**33.91**

Table 8.3: Cost associated to electrical consumption

Also in this section the cost of internet access will be regarded, taking into account that the monthly cost of said access is set at 29.95€. In Table 8.4 the cost is computed with the hours dedicated to the project.

	Usage time (h)	Unitary cost (€/h)	Subtotal (€)
Internet access	300	0.042	**12.48**

Table 8.4: Cost associated to internet access

8.4 Software costs

The cost of the software that has been employed is detailed in Table 8.5.

The programs Word, Excel and Power Point are all part of the Microsoft Office 365 family of software, as well as the Teams tool. The university pays 79 €for a 4 year license for each student.

In the case of the CFD software ANSYS in which the simulations themselves have been performed, a power-on-demand license has been used, with a cost of 0.80€/h and a total of 200 h of usage.

LaTeX has been the software used for the elaboration of the present document, and it can be found online as a free tool.

Fusion 360 has been used for the elaboration and dimensioning of certain sketches, and it has been obtained via the free educational plan of Autodesk.

Finally, MATLAB has been employed for the post processing of the data obtained in the simulations. The cost of a yearly educational license is of 250€, which has been split as a monthly cost and computed according to the duration of the project.

	Cost	Usage time	Subtotal (€)
Microsoft Office 365	1.65€/month	8 months	13.20
ANSYS	0.80€/h	200 h	160
LaTeX	Free	-	-
Fusion 360	Free	-	-
MATLAB	20.83€/month	8 months	166.67
		Total	**339.87**

Table 8.5: Cost associated to the software

8.5 Total cost

The total cost of the project is shown in Table 8.6, with a 21% of VAT applied to the subtotal cost:

	Cost (€)
Human resources	2772
Equipment	16.67
Electrical consumption	33.91
Internet access	12.48
Software	339.87
Subtotal	3174.93
VAT (21%)	666.74
TOTAL	**3841.67**

Table 8.6: Total cost of the project

8. Bibliography

[1] Croatian journal of forest engineering. Volume 42, issue 1, 2021.

[2] Shaik Amjad, S. Neelakrishnan, and R. Rudramoorthy. Review of design considerations and technological challenges for successful development and deployment of plug-in hybrid electric vehicles. *Renewable and Sustainable Energy Reviews*, 14(3):1104 – 1110, 2010.

[3] ANSYS. Ansys fluent tutorial guide 2020 r2 - 26. simulating a 1p3s battery pack using the battery model, July 2020. Accessed July 15, 2021.

[4] ANSYS. Fluent theory guide 2020 r2 - 24.2.1. battery solution methods, 2021. Accessed July 15, 2021.

[5] ANSYS. Fluent theory guide 2020 r2 - 24.2.2. electro-chemical models, 2021. Accessed July 15, 2021.

[6] ANSYS. Fluent user's guide 2020 r2 - 32.3.4. setting up the battery model, 2021. Accessed July 15, 2021.

[7] Shashank Arora. Selection of thermal management system for modular battery packs of electric vehicles: A review of existing and emerging technologies. *Journal of Power Sources*, 400:621 – 640, 2018.

[8] Bharat Balagopal and Mo-Yuen Chow. Effect of anode conductivity degradation on the thevenin circuit model of lithium ion batteries. 10 2016.

[9] Todd Bandhauer, Srinivas Garimella, and Thomas Fuller. A critical review of thermal issues in lithium-ion batteries. *Journal of The Electrochemical Society*, 158:R1, 01 2011.

[10] K.T Chau, Y.S Wong, and C.C Chan. An overview of energy sources for electric vehicles. *Energy Conversion and Management*, 40(10):1021 – 1039, 1999.

[11] Mehmet Cuma, Emrah Yirik, Cagla Unal, Erdem Ünal, Burak Onur, and Mehmet Tümay. Design considerations of high voltage battery packs for electric buses. *INTERNATIONAL JOURNAL OF ADVANCES ON AUTOMOTIVE AND TECHNOLOGY*, 01 2017.

[12] Marc Doyle, Thomas F. Fuller, and John Newman. Modeling of galvanostatic charge and discharge of the lithium/polymer/insertion cell. *Journal of The Electrochemical Society*, 140(6):1526–1533, jun 1993.

[13] Ali Eftekhari. Low voltage anode materials for lithium-ion batteries. *Energy Storage Materials*, 7:157 – 180, 2017.

[14] Javad Esmaeili and Hamid Jannesari. Developing heat source term including heat generation at rest condition for lithium-ion battery pack by up scaling information from cell scale. *Energy Conversion and Management*, 139:194–205, 2017.

[15] Berdichevsky G, Kelty K, Straubel JB, and Toomre E. The tesla roadster battery system. 2006.

[16] Cary M. Hayner, Xin Zhao, and Harold H. Kung. Materials for rechargeable lithium-ion batteries. *Annual Review of Chemical and Biomolecular Engineering*, 3(1):445–471, 2012. PMID: 22524506.

[17] S. S. Madani, M. J. Swierczynski, and S. K. Kær. The discharge behavior of lithium-ion batteries using the dual-potential multi-scale multi-dimensional (msmd) battery model. In *2017 Twelfth International Conference on Ecological Vehicles and Renewable Energies (EVER)*, 2017.

[18] Min Chen and G. A. Rincon-Mora. Accurate electrical battery model capable of predicting runtime and i-v performance. *IEEE Transactions on Energy Conversion*, 21(2):504–511, 2006.

[19] Naoki Nitta, Feixiang Wu, Jung Tae Lee, and Gleb Yushin. Li-ion battery materials: present and future. *Materials Today*, 18(5):252 – 264, 2015.

[20] Scott P and Burton M. The new bmw i3, 2013. `http://www.asymcar.com/graphics/14/i3/bmwi3b.pdf`. Accessed July 15, 2021.

[21] H. Qiao and Q. Wei. 10 - functional nanofibers in lithium-ion batteries. In Qufu Wei, editor, *Functional Nanofibers and their Applications*, Woodhead Publishing Series in Textiles, pages 197 – 208. Woodhead Publishing, 2012.

[22] Sigma-Aldrich. Battery principles and conventional materials. `https://www.sigmaaldrich.com/materials-science/material-science-products.html?TablePage=106039040`. Accessed July 15, 2021.

[23] Peyman Taheri, Scott Hsieh, and Majid Bahrami. Investigating electrical contact resistance losses in lithium-ion battery assemblies for hybrid and electric vehicles. *Lancet*, 196:6525–6533, 08 2011.

[24] MIT Electric Vehicle Team. A guide to understanding battery specifications. December 2008. `http://web.mit.edu/evt/summary_battery_specifications.pdf`. Accessed July 15, 2021.

[25] Toshiba. Toshiba scib rechargeable battery catalog, 2010. `https://www.scib.jp/en/download/ToshibaRechargeableBattery-en.pdf`. Accessed July 15, 2021.

[26] Qian Wang, Bin Jiang, Bo Li, and Yuying Yan. A critical review of thermal management models and solutions of lithium-ion batteries for the development of pure electric vehicles. *Renewable and Sustainable Energy Reviews*, 64:106 – 128, 2016.

[27] Reza Younesi, Gabriel M. Veith, Patrik Johansson, Kristina Edström, and Tejs Vegge. Lithium salts for advanced lithium batteries: Li–metal, li–o2, and li–s. *Energy Environ. Sci.*, 8:1905–1922, 2015.